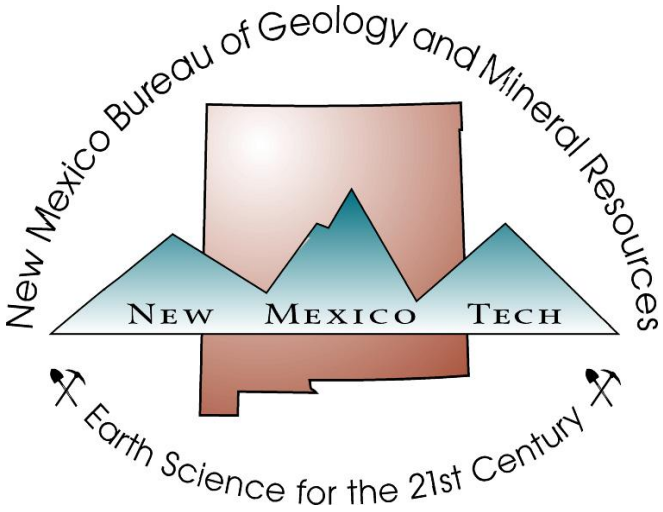

Additional analyses and mapping of the Hubbell Spring and other intrabasin faults south of Albuquerque, New Mexico

by

Susan S. Olig and Judith Zachariasen

New Mexico Bureau of Geology and Mineral Resources, New Mexico Tech
Socorro, New Mexico 87801

Open-file Report 527

May, 2010

ADDITIONAL ANALYSES AND MAPPING OF THE HUBBELL SPRING AND OTHER INTRABASIN FAULTS SOUTH OF ALBUQUERQUE, NEW MEXICO

Final Report

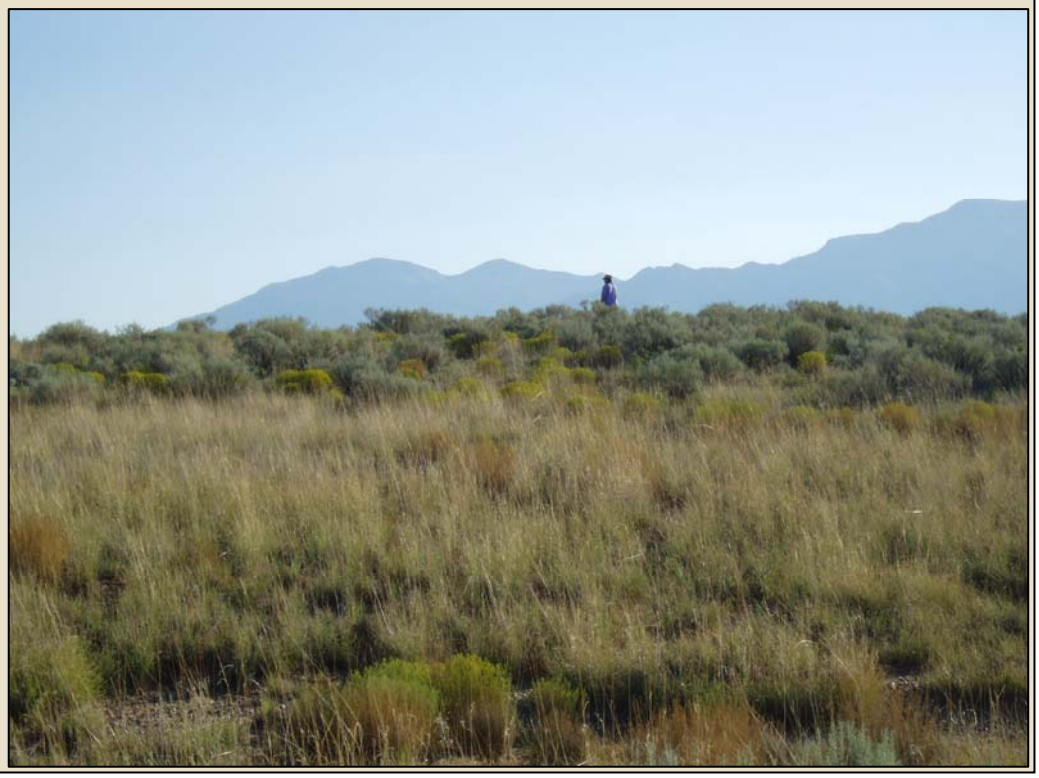

URS Corporation
Job No. 26814877

USGS NEHRP Award No.
04HQGR0079

ADDITIONAL ANALYSES AND MAPPING OF THE HUBBELL SPRING AND OTHER INTRABASIN FAULTS SOUTH OF ALBUQUERQUE, NEW MEXICO

Submitted to:

U.S. Geological Survey
National Earthquake Hazards Reduction Program
Award No. 04HQGR0079

Submitted by:

Susan S. Olig and Judith Zachariasen
URS Corporation
500 12th Street, Suite 200
Oakland, CA 94607
Ph: (510) 874-1729
FAX: (510) 874-3268
Email: susan_olig@urscorp.com

April 14, 2008

Research supported by the U.S. Geological Survey (USGS) Department of the Interior, under USGS award number 04HQGR0079. The views and conclusions contained in this document are those of the authors and should not be interpreted as necessarily representing the official policies, either expressed or implied, of the U.S. Government.

Job No. 26814877

The Hubbell Spring fault system (HSFS) is an active, normal fault system near the eastern margin of the Albuquerque-Belen basin in the central Rio Grande rift. Previous mapping suggested that the HSFS includes 3-4 major splays. Trenching studies indicated that multiple late Quaternary events had large displacements ranging from 1.7 to 4.7 m, implying longer rupture lengths than previously mapped (~43 km). We conducted additional mapping to the south on the southern Llano de Manzano surface and found that several previously unnamed faults connect with the HSFS, resulting in a ≈ 74-km long fault system. We also identified numerous previously unmapped late Quaternary fault splays, some of which are tens of kilometers long and have scarps over 10 m high. Almost all of the splays show down-to-the west displacement except a couple of prominent faults to the south near Abo Arroyo. Based on our mapping, the HSFS is characterized by an unusually broad deformation zone (as wide as 18 km, but typically 10-14 km) of subparallel, anastomozing and branching normal faults that strike north-south overall, typically dip west, and offset late Quaternary eolian and piedmont deposits down to the west. The geometry of fault traces and the along-strike displacement variation patterns suggest complex patterns of slip transfer between fault splays of the HSFS, with northwest- and northeast-striking sections serving as relay ramps between principal north-south striking faults. Additional study is needed to better quantify these deformation patterns.

Unlike typical normal faults, the HSFS generally lacks antithetic faults or backtilting in the hanging wall. Rather, many splays are characterized by backtilt to the east of the footwall resulting in closed depressions developing on the upthrown side of the scarp. We measured two long topographic profile transects across the HSFS. Backtilting in the footwall results in large uncertainties for displacement estimates. Vertical surface displacements across individual scarps range from 0 to 31 meters. The cumulative vertical surface displacement is about 28-54 m and 41-83 m across the northern and southern transects, respectively. Assuming an age of 80-130 ka for the faulted surface, we obtain cumulative average vertical slip rates of 0.2-0.7 mm/yr for the northern transect and 0.3 to 1.0 mm/yr for the southern transect, making the HSFS the longest, most active fault system near Albuquerque. These slip rates are much higher than previous estimates due to the newly discovered fault traces. Several other fault systems in the Rio Grande rift show similar distributed, anastomozing geometries, but the footwall backtilting is unusual and requires further investigation.

As a minor component of this study we also analyzed three additional luminescence samples (CHSF02-2, CHSF02-9, and CHSF02-11) previously collected from the Carrizo Spring trench on splay L, or the central HSFS (Olig et al., 2004). Results of the additional analyses are consistent with the previous results from 8 samples and help substantiate previous age estimates for the youngest and oldest faulting events, which respectively occurred shortly before 5 to 6 ka, and between 65 and 84 ka. These additional age analyses also help substantiate the average late Quaternary slip rate estimate of 0.09 ± 0.01 mm/yr for splay L of the HSFS (Olig et al., 2004).

Cover Photographs:

Top – Looking east at fault splay G-H of the Hubbell Spring fault system, east of Las Maravillas. Scarp is about 12 m high. To the north, this fault splay likely connects to the Palace-Pipeline fault of Maldonado et al. (1999; 2007).

Bottom – Looking east-northeast at a 3-m-high scarp near the southern end of fault splay J of the Hubbell Spring fault system (formerly known as the Western Hubbell Spring fault of Maldonado et al., 1999; 2007).

TABLE OF CONTENTS

List of Figures

List of Tables

Plate

Acknowledgements

This study was funded by the U.S. Geological Survey (USGS) through a National Earthquake Hazard Reduction Program Award (No. 04HQGR0079), with support for report preparation from the URS Professional Development Fund. We thank Michael Timmons, Geoffrey Rawling, David McCraw, Sean Connell, and Dave Love (New Mexico Bureau of Geology and Mineral Resources [NMBGMR]) for sharing mapping data and Tien Grauch (USGS) for sharing aeromagnetic results. Michael Machette (USGS) generously loaned aerial photographs. Melinda Lee (URS) assisted with report preparation.

The greater metropolitan area of Albuquerque, New Mexico has a population exceeding 700,000 and is one of the fastest growing urban areas in the western U.S. The Hubbell Spring fault is one of the most active faults in the Albuquerque basin (Personius et al., 1999; Figure 1). It is the most significant seismic source to the southern Albuquerque area, particularly to the rapidly growing communities of Los Lunas and Belen (Wong et al., 2000). Previous mapping by Machette and McGimsey (1983) indicated that the Hubbell Spring fault was 43 km long with one main splay. In contrast, recent mapping of the northern portion in the Isleta Pueblo (e.g., Love et al., 1996; Love, 1998; Maldonado et al., 1999) suggested the presence of additional principal fault splays, whereas geophysical (e.g., Grauch, 2001; Sweeney et al., 2002) and recent paleoseismic (Olig et al., 2004, 2005, in review) studies suggested longer lengths for the Hubbell Spring fault, raising significant questions about the extent of late Quaternary ruptures to the south and the relation of the Hubbell Spring fault to nearby faults.

1.1 PURPOSE AND SCOPE

The purpose of this study was two-fold: (1) conduct three additional luminescence analyses of samples collected during a previous paleoseismic trench investigation (Olig et al., 2004); and, (2) conduct more detailed mapping of late Quaternary fault scarps south of the Isleta Pueblo, in order to better define the extent and geometry of the Hubbell Spring fault. In this study, we identified several newly discovered subparallel anastomosing faults and extended some previously mapped faults farther to the south, resulting in a total width of faulting of as much as 18 km and a total length of nearly 74 km (Plate 1). To better reflect this greater extent and complexity, we herein refer to these faults as the Hubbell Spring fault system (HSFS).

1.2 GEOLOGIC SETTING

The HSFS is a north-striking, west-dipping, system of intrabasin normal faults that lies near the eastern margin of the Albuquerque basin in the central Rio Grande rift of New Mexico (Figure 1). The rift is a physiographic and structural depression that is now recognized as a continental rift zone (e.g., Keller and Cather, 1994). It consists of a series of north trending, *en echelon* structural basins that are flanked by mountain ranges or uplifted plateaus, extending for about 1,000 km from central Colorado, through central New Mexico, and into west Texas and Mexico (Chapin, 1971). The namesake river, the Rio Grande, follows this seismically, tectonically and volcanically active depression, which is actually part of the Basin and Range Province (Hawley, 1986). The Rio Grande rift is characterized by: (1) late Cenozoic extension accommodated by faulting and volcanism that is as young as Holocene; (2) shallow ($\leq$ 13 km) diffuse background seismicity that generally is not associated with specific structures except for some zones that may be correlated with magmatic activity; (3) focal mechanisms that indicate a mix of normal and strike-slip faulting, and a horizontal least principal stress direction of WNW-ESE; (4) high heat flow; (5) deep asymmetric half grabens, and grabens that tend to show opposing symmetries (tilting to the west versus tilting to the east); and (6) large negative gravity anomalies (Chapin and Cather, 1994; Keller and Cather, 1994; Morgan et al., 1986; Sanford et al., 1991).

The Albuquerque basin is nearly 120 km long, 40 to 60 km wide, and is the largest and deepest rift basin in New Mexico (Hawley et al., 1995; Connell, 2004). Clastic deposits (alluvial, colluvial, eolian, lacustrine and volcaniclastic sediments) and volcanic rocks comprise the Santa Fe Group, the Plio-Pleistocene syn-rift sedimentary fill of Rio Grande rift basins (e.g. Hawley et

al., 1969; Connell, 2004). These basin fill deposits are as thick as 4,570 m (≈15,000 ft) in the Albuquerque basin (Hawley et al., 1995). Although extension in the region initiated 27 to 32 Ma, rift basins were not integrated by the through-going ancestral drainage of the Rio Grande until much later. The axial fluvial and tributary deposits of the ancestral Rio Grande in the Albuquerque basin are part of the Sierra Ladrones Formation of Machette (1978), and were deposited from 7 Ma to sometime after 1.2 Ma (Connell et al., 2001). The top of these deposits formed a Pleistocene basin floor that is now 100 to 200 m above the present Rio Grande, indicating substantial subsequent incision that left extensive alluvial surfaces abandoned (Machette and McGimsey, 1983; Machette, 1985). Based on recent mapping and stratigraphic studies, Connell et al. (2001) estimate that the Rio Grande initiated this incision sometime between 0.7 and 1.2 Ma.

The Albuquerque basin is flanked on the east by the east-tilted, fault-block uplift of the Sandia, Manzanita, Manzano and Los Piños Mountains (Kelley, 1977). These ranges expose Precambrian plutonic and metamorphic rocks that are unconformably overlain by Paleozoic limestones, sandstones and shales. The resulting structural relief is as much as 8,500 m (Woodward 1982). The basin is flanked to the west by the lower-relief uplifts of the Colorado Plateau. Based on seismic lines, drill holes and gravity data, Lozinsky (1994) and Russell and Snelson (1994) separated the Albuquerque basin into two subbasins: one north of Tijeras Canyon with at least 17% extension and basin fill tilted to the east, and a subbasin to the south of Los Lunas (including most of the HSFS) that has 30% extension and basin fill sediments dominantly tilted to the west. They postulated that the Tijeras accommodation zone, a buried west-southwest extension of the Tijeras-Canoñcito fault system, separated these subbasins. However, subsequent investigators (Maldonado et al., 1999, 2007), following Hawley et al. (1995), have suggested that a buried northwest-trending structure, the Mountain View fault zone, likely separates the subbasins. Based on gravity studies, Grauch (1999) separated the Albuquerque basin into three sub-basins: the Santo Domingo, Calabacillas and Belen. Regardless, the HSFS lies within the Albuquerque basin about 3 to 10 km west of the basin-bounding Manzano fault (#2118 on Figure 1) and appears to transect both the Belen and Calabacillas sub-basins. The HSFS cuts the Tijeras-Cañoncito fault system (#2033) near its northern end and lies along-strike of the less-active Sandia fault (#2037) to the north (Figure 1). Note that as defined here, the HSFS also includes the newly discovered Palace-Pipeline fault (Love, 1998; Maldonado et al., 1999) that is located a few kilometers east of Los Lunas (Figure 2) and connects with a major trace of the McCormick Ranch faults (#2135 on Figure 1).

Although the HSFS is an intrabasin structure, its structural relief, prominent geomorphic expression, and relation to adjacent faults suggest it currently forms the active rift margin (Machette and McGimsey, 1983). For example, Permian, Triassic and Tertiary rocks are exposed in some portions of the footwall of the HSFS (in particular of splay L), indicating unusually substantial structural relief across this intrabasin fault (Reiche, 1949; Kelley, 1977; Love et al., 1996; Rawling and McCraw, 2004). Stark (1956) estimated a total throw of ≈2,256 m (7,400 ft) across the central HSFS based on footwall bedrock exposures and logs of the Grober No. 1 well that he thought bottomed in the Triassic Chinle Formation on the downthrown side of the fault. However, Hudson and Grauch (2003) reinterpreted this drill hole and concluded it bottomed in Neogene basin fill, not the Chinle Formation, which suggests that the total throw is likely greater. Additionally, the HSFS is most closely associated with a strong north-south trending gravity gradient along the Hubbell Bench (Figure 2), and recent gravity and

aeromagnetic modeling studies suggest that the major basement offset is a little more than 2 km west of the central splay, or our splay L, of the HSFS (Grauch and Hudson, 2002). Finally, and most importantly, although fault scarps are scarce along the Manzano fault (Machette et al., 1998), late Quaternary fault scarps of the HSFS are evident along most of the Llano de Manzano, an early to late Pleistocene alluvial surface that extends for over 90 km south of Albuquerque between the Rio Grande to the west and the Manzano Mountains to the east (Figure 1).

The Llano de Manzano is a gently west-sloping surface (Figure 1) that was considered by Machette (1985) to be graded to an alluvial terrace that lies 92 to 113 m above the modern Rio Grande. Based on soil studies and geomorphic and stratigraphic relations, he estimated an age on the order of about 300 ka. Based on more recent detailed mapping and stratigraphic studies, Maldonado et al. (1999) broke out two additional older surfaces, the Sunport and Cañada Colorado, north of Hells Canyon Wash. They estimate a Pliocene age for the Cañada Colorado and early Pleistocene ages for the Sunport and Llano de Manzano surfaces. As an extension of these studies, Connell et al. (2001) consider the Llano de Manzano actually to consist of multiple surfaces of a basin fill succession that includes early Pleistocene piedmont deposits shed off the Manzano Mountains, overlying and truncating ancestral axial Rio Grande deposits. They provisionally assign these upper Santa Fe Group deposits to the Sierra Ladrones Formation of Machette (1978). Deposition of these basin fill deposits is thought to have ended between 0.7 and 1.2 Ma, when the Rio Grande began incising down to its present channel position. Blanketing most of the Llano de Manzano are late Quaternary eolian cover sands, dunes and piedmont alluvium. Thus, as we use it here, the Llano de Manzano surface includes these younger eolian and alluvial deposits. The eolian sands are particularly significant to fault studies because they tend to dominate over colluvial sedimentation along faults (e.g., Personius and Mahan, 2003), they complicate age estimates of the many alluvial surfaces in the region, they can mute the geomorphic expression of faults, and they are excellent candidates for luminescence dating. For example, luminescence ages for eolian sands exposed in previous paleoseismic studies range in age from 5 to 85 ka (Personius and Mahan, 2003; Olig et al., 2004). Still, despite the eolian cover, scarps of the HSFS are as high as 40 m on the Pliocene Cañada Colorado and as high as 25 m on the Pleistocene Llano de Manzano (Machette and McGimsey, 1983), forming a prominent and fairly continuous late Quaternary fault system south of Albuquerque.

1.3 PREVIOUS STUDIES

Read et al. (1944) first mapped the HSFS and named it the Ojuelos fault for Los Ojuelos Springs. Several early investigators also used this name (e.g., Reiche, 1949; Stark, 1956; Titus, 1963), but through time “Hubbell Spring(s)” was added, or replaced “Ojuelos” in the name (e.g., Kelley, 1977; Machette, 1982; Machette and McGimsey, 1983), and so Machette et al. (1998) used the name Hubbell Spring fault, and we partially retain that nomeclature here, upgrading this long and complex zone with several subparallel major strands to a fault system.

Machette and McGimsey (1983) were the first to focus on mapping, profiling and analyzing Quaternary fault scarps of the HSFS, describing them as “perhaps the most spectacular fault scarps in the central Rio Grande rift.” They mapped an anastomozing series of three dominant splays that converged to the north and had a total length of 34 (their text and Table 2) to 43 (their map) km, with only the central trace extending south of Los Lunas (Figure 1). They measured scarp heights of 2 to 40 m on Pliocene to late Pleistocene deposits, with larger offsets on older

surfaces clearly indicating recurrent Quaternary movements. Reiche (1949) suggested movement was youngest along the southern portion and possibly Holocene. Based on their morphometric analyses, Machette and McGimsey (1983) also concluded movement was younger to the south, breaking the fault into northern and southern segments. However, based on comparison to 5-ka and 15-ka scarps studied elsewhere in the Basin and Range, they concluded that youngest faulting on the HSFS was late Pleistocene, but probably considerably older than 15 ka.

More recent detailed mapping of late Cenozoic sediments along the northern HSFS in the Isleta Pueblo (e.g., Love et al., 1996; Love, 1998; Maldonado et al., 1999) suggests that the fault geometry of the northern HSFS is even more complex and some traces are much longer than previously mapped by Machette and McGimsey (1983; cf. Figures 1 and 3). In particular, Maldonado et al. (1999) mapped several anastomosing, discontinuous fault traces that still form three dominant north-south trending fault splays, (which they referred to as western, central and eastern Hubbell Spring faults), but how they merge together to the north is mapped differently than by Machette and McGimsey (c.f., Figures 1 and 3). Additionally, Machette and McGimsey (1983) showed the western and eastern traces dying out northeast of Los Lunas (Figure 1), whereas Maldonado et al. (1999) extend these traces at least another 15 kilometers to the south (Figure 2). Although Maldonado et al. (1999) mapped the three splays of the HSFS extending south of Hells Canyon, the eastern splay is somewhat enigmatic as it appears to show down-to-the-east offset in the subsurface south of Hells Canyon (V. S. Grauch, personnal communication, 2005) where it has no surface expression, but has a down-to-the-west scarp north of Hells Canyon. Maldonado et al. (2007) have reinterpreted this down to the east southern portion as a separate buried fault that they named the Meadow Lake fault. Despite the prominent aeromagnetic signature of the Meadow Lake fault (Figure 3), it has a poor geomorphic expression (we found no associated fault scarps south of Hells Canyon), no associated gravity gradient (Figure 2), and may actually be a relict fault from a pre-Quaternary period of extension. As such, the Meadow Lake fault may have a longer, more complicated kinematic history than the rest of the HSFS, with only the northern portion (eastern HSFS splay) having been reactivated during Pleistocene extension.

Another recent revision to the mapping of the HSFS is the inclusion of the newly identified Palace-Pipeline fault (Love, 1998; Maldonado et al., 1999), a zone of faults located just west of the western HSFS (Figure 2), which was not included in the Quaternary fault compilation of Machette et al. (1998) (Figure 1). Nonetheless, its close proximity, similar geometry and geomorphic expression to the HSFS suggest it may be another anastomozing trace of the HSFS. This fault strikes north-south and offsets the Pleistocene Sunport and Llano de Manzano surfaces down to the west by as much as 15 m (Maldonado et al., 1999). North of Hells Canyon Wash, the Palace-Pipeline fault connects with one of the main traces of the McCormick Ranch faults (#2135 on Figure 1) as mapped by Love et al. (1996) and Maldonado et al. (1999) (Figure 2; Maldonado et al., 2007). The McCormick Ranch faults include several anastomozing west- and east-facing fault scarps (GRAM Inc. and WLA, 1995) offsetting the older Sunport surface overall down to the west. Maldonado et al. (1999; 2007) extended the Palace-Pipeline fault at least as far south as El Cerro Tome, making it a minimum of 18 km long. Drill-hole data indicate that there is a much thicker package (.5 km) of Plio-Peistocene Santa Fe Group sediments on the downthrown side of the Palace-Pipeline fault (Figure 4 of Maldonado et al., 1999). This suggests that this fault may have been the most active splay of the HSFS during earlier rifting. However, Maldonado et al. (2007) revised this interpretation so that most of displacement is inferred to have occurred on the buried Mountain

View fault, which is an inferred, older, lower-angle, normal fault that is slightly offset by the Palace-Pipeline fault. The Palace-Pipeline fault corresponds to our fault splay H (Plate 1).

Recent airborne aeromagnetic surveys (Grauch, 2001; Sweeney et al., 2002) support Maldonado et al.'s mapping and suggest that the Palace-Pipeline fault and the western splay of the HSFS potentially extend even farther south, up to 45 kilometers or more, and are as long as the central HSFS (Figure 3). Indeed, mapping from this study shows that late Quaternary fault scarps of the HSFS do extend much farther south than previously recognized. They are fairly continuous to Abo Arroyo, and even extend as far south as Black Butte, forming a complex fault system that is roughly 74 km long (Plate 1).

Two paleoseismic trench investigations have been conducted on the HSFS. The first study was across a 7-m-high scarp on the western HSFS (most likely a continuation of our fault splay J) near Hubbell Spring at its northern end (Figure 1, Plate 1). The trench revealed evidence for four surface-faulting events that occurred since deposition of fan deposits on the Llano de Manzano (Personius et al., 2001) probably around 92 ± 7 ka (Personius and Mahan, 2003). These events resulted in 5 to 8 m of throw and average displacements per event of 1 to 2 m (Personius et al., 2001). The luminescence ages of colluvial /eolian deposits associated with faulting indicate that the most recent, penultimate and antepenultimate events occurred around 12 ± 1 ka, 29 ± 3 ka, and 56 ± 6 ka, respectively (Personius and Mahan, 2003). The age of the oldest event is poorly constrained but it occurred prior to the antepenultimate event and some time after 92 ± 7 ka.

More recently, Olig et al. (2004, 2005, in review) completed a paleoseismic investigation of the central HSFS (which is our fault splay L) at the Carrizo Spring trench site (Figures 1 and 2). They excavated a trench and soil pit, and drilled three shallow borings, which exposed piedmont alluvium, slopewash colluvium, playa deposits, eolian sands, and several buried soils throughout the section (Figure 4). They broke out 14 stratigraphic units (units 1 through 14 on Figure 4) and 7 buried soils in the trench. The excavations and borings revealed structural, stratigraphic, and pedologic evidence for at least 4, probably 5, large earthquakes that occurred since deposition of piedmont alluvium (Unit 1b on Figure 4) on the Llano de Manzano about 83.6 ± 6.0 ka (Olig et al., 2004). The total down-to-the-west throw on these deposits was 7.3 ± 0.5 m, yielding a late Quaternary slip rate of 0.09 ± 0.01 mm/yr for the central HSF. Displacements per event ranged from 0.4 to 3.7 m, with a preferred average of 1.5 m.

Olig et al. (2004) collected 11 samples for infrared-stimulated luminescence (IRSL) analyses to provide absolute ages; however, they only had funding to analyze 8 samples. Those 8 samples were all stratigraphically consistent within 1 σ, and multiple analyses from the same unit overlapped within 1 σ. Overall the stratigraphic relations and ages indicate the following timing of events (from youngest, Z, to oldest, V):

(1) Z – occurred shortly before 6 ka and well after 27 ka;

(2) Y – occurred before event Z and after 27 ka;

(3) X – occurred shortly before 26.8 ± 2.4 ka and after 30.2 ± 2.2 ka;

(4) W – occurred before 30.2 ± 2.2 ka and well after 65 ± 6 ka; and

(5) V – occurred before 65 ± 6 ka and well after 83.6 ± 6.0 ka.

Thus, the ages of the 4 largest events (Events V, W, X, and Z) on the central HSFS (our splay L) overlap with the ages of the 4 latest events on the western HSFS (most likely our splay J). Figure 5 shows a comparison of the paleoseismic records for the two trench sites. The overlap of ages, along with the relatively large displacements per event, is suggestive but not conclusive of coseismic rupture of the western and central splays of the HSFS (Olig et al., 2004; in review). Estimated vertical displacement per event range from 1.7 m to 4.7 m for coseismic rupture of fault splays J and L, which are unusually large for a 43-km-long surface rupture (Olig et al., 2004; in review), which was also suggestive that the HSFS is indeed longer than previously mapped.

To supplement age analyses conducted by Olig et al. (2004), we analyzed three additional luminescence samples (CHSF02-2, CHSF02-9, and CHSF02-11) collected from the Carrizo Spring trench on the central HSFS (our splay L). The locations of these samples are shown on Figure 4 and results of the analyses are shown in Table 1. Our sampling and analyses methods are described in Olig et al. (2004; in review).

Results of the additional analyses are consistent with the previous results of Olig et al. (2004). As expected, they do not tighten age constraints, but they do help corroborate previous age estimates for surface-faulting events on splay L of the HSFS. Specifically, samples CHSF02-11 and CHSF02-09 yielded ages of 5.3 ± 0.4 and 5.4 ± 0.4 ka, respectively. These ages help substantiate that a package of eolian-dominated sediments (units 11 through 13) were rapidly deposited around 5 to 6 ka, after the most-recent surface faulting event, Z, occurred on splay L of the HSFS (Figure 5). Sample CHSF02-02 was from a sag pond deposit (Unit 2) that post-dates the oldest faulting event, V, and yielded an age of > 59.1 ± 4.5. This is consistent with a previous age estimate of 65.2 ± 5.6 for Unit 2 (Table 1). Overall, the additional ages help substantiate previous age estimates (as discussed on page 1-5 and shown on Figure 5) and also the average late Quaternary slip rate estimate of 0.09 ± 0.01 mm/yr for splay L of the HSFS (Olig et al., 2004).

Table 1
Luminescence Age Data for the Carrizo Spring Trench Across Fault Splay L of the Hubbell Spring Fault System[1]

Field No.[2]	Lab Sample No.	Stratigraphic Unit	U (ppm)	Th (ppm)	K_20 (%)	Polymineral IRSL 4-11 μ De (Grays)	Moisture Content (%)	Dose Rate (Grays)[3]	IRSL or OSL Age (ka)[4]	Comments
CHSF02-11	***UIC1357***	***Unit 14 Eolian sand***	***2.51 ±0.45***	***8.80 ±1.24***	***2.05 ±0.02***	***16.88 ±0.06***	***5 ±2***	***3.20 ±0.15***	***5.3 ±0.4***	***Post-dates Event Z***
CHSF02-10	UIC1088	Unit 13 Eolian sand	2.55 ± 0.41	8.08 ± 1.16	2.16 ± 0.02	24.30 ± 0.18	5 ± 2	4.02 ± 0.19	**6.0 ± 0.4**	Post-dates Event Z
CHSF02-8	UIC1056	Unit 11 Scarp-derived slopewash colluvium	3.53 ± 0.40	6.42 ± 0.75	2.13 ± 0.02	22.66 ± 0.24	5 ± 2	3.66 ± 0.17	**5.5 ± 0.4**	Post-dates Event Z
CHSF02-9	***UIC1358***	***Unit 11 Scarp-derived slopewash colluvium***	***3.82 ±0.46***	***8.41 ±1.23***	***2.13 ±0.02***	***19.22 ±0.04***	***5 ±2***	***3.56 ±0.17***	***5.4 ±0.4***	***Post-dates Event Z***
CHSF02-5	UIC1054	Unit 6 Loess	6.14 ± 0.59	9.64 ± 1.31	1.98 ± 0.02	124.84 ± 0.82	5 ± 2	4.47 ± 0.20	**24.9 ± 1.7**	Post-dates Event X and pre-dates Event Y(?)
CHSF02-7	UIC1089	Unit 6 Loess	5.76 ± 0.76	11.29 ± 2.06	2.05 ± 0.02	158.90 ± 1.12	5 ± 2	5.44 ± 0.22	**28.7 ± 2.4**	Post-dates Event X and pre-dates Event Y(?)
CHSF02-6	UIC1055	Unit 4 Eolian sand	3.09 ± 0.43	7.78 ± 1.19	1.93 ± 0.02	122.12 ± 0.48	5 ± 2	3.60 ± 0.16	**30.2 ± 2.2**	Post-dates Event W
CHSF02-1	UIC1091	Unit 2 Sag pond deposit	5.58 ± 0.75	11.29 ± 2.09	2.46 ± 0.02	362.43 ± 1.12	10 ± 3	5.56 ± 0.23	**65.2 ± 5.6**	Post-dates Event V and pre-dates Event W
CHSF02-2	***UIC1359***	***Unit 2 Sag pond deposit***	***4.19 ±0.58***	***12.55 ±1.56***	***2.10 ±0.02***	***267.21 ±2.01***	***10 ±3***	***4.52 ±0.20***	***> 59.1 ±4.5***	***Post-dates Event V***
CHSF02-3	UIC1090	Unit 1b Eolian sand	3.10 ± 0.36	5.00 ± 0.91	2.02 ± 0.02	300.34 ± 2.97	10 ± 3	3.56 ± 0.16	**84.6 ± 6.0**	Pre-dates Event V and buried soil, S_l, on Llano de Manzano
CHSF02-4	UIC1053	Unit 1b Slopewash	2.86 ± 0.38	7.21 ± 1.09	2.14 ± 0.02	315.00 ± 1.16	10 ± 3	3.60 ± 0.17	**82.5 ± 6.0**	Pre-dates Event V and and S_l on Llano de Manzano

[1] Additional analyses done for this study are shown in ***bold/italics***. Previous analyses are from Olig et al., 2004. All samples are listed in stratigraphic order. Samples CHSF02-9 and CHSF02-11 were green optically stimulated luminescence (OSL) analyses, all others were infrared stimulated luminescence (IRSL) analyses with measurements made using a multiple aliquot additive dose (MAAD) method, measuring blue emissions on the 4 to 11 micron polymineral fraction. See Olig et al. (2004) for more details.

[2] Sample locations shown on Figure 4. Trench location shown on Figure 1 and Plate 1.

[3] All errors are at one sigma and calculated by averaging the errors across the temperature range.

[4] Ages are rounded to the nearest 100 years and all errors are at one sigma.

3.1 METHODS

The study area for our mapping extended from the base of the Manzano Mountains on the east, to the western edge of the Llano de Manzano on the west, and between the Isleta Pueblo on the north, and the Sevilleta National Wildlife Refuge on the south (Plate 1). This area covered roughly 1,200 km^2, (11 7.5' quadrangles) and included the counties of Bernalillo, Valencia, Socorro, and Torrance. Due to access restrictions, we generally did not field check areas in the pueblo or refuge. Due to time restrictions, we did not consistently check exposures below the eastern edge of Llano de Manzano for faults. We also did not map fault scarps of the Manzano or Los Piños faults, which are range front faults along the base of the Manzano and Los Piños Mountains, respectively (Figure 1, Plate 1).

We mapped Quaternary fault scarps offsetting unconsolidated sediments on the Llano de Manzano surface. These sediments are dominantly Pleistocene to Holocene alluvium, colluvium, eolian cover sands and dunes overlying Plio-Pleistocene basin-fill deposits. Piedmont alluvium on the Llano de Manzano includes broad gently sloping aprons and relatively steep, but localized, fan deposits present along the base of the Manzano and Los Piños Mountains. Additionally, localized playa deposits are also evident, particularly in closed-depressions along fault scarps.

The mapping portion of our study included: (1) review of previous studies and existing data including topographic and geologic maps, studies discussed in Section 1.2, DEM data (10-m resolution), and orthophoto quadrangles; (2) interpretation of black and white stereo aerial photographs at different scales (≈1:41,000-scale 1996 NAPP, and some ≈1:52,000-scale 1953 AMS photographs) to identify fault scarps and selected geomorphic features on overlays; (3) reconnaissance and detailed field checking of aerial photograph interpretation; (4) topographic profiling of fault scarps along two long transects (P1 and P2 on Plate 1) across the HSFS; and (5) data analysis and production of a 1:100,000-scale GIS-based map and this report (Plate 1).

We profiled fault scarps along two transects across the HSFS (Plate 1). The purpose of these transects was to: (1) quantify the cumulative down-to-the-west net vertical surface offset of the Llano de Manzano surface across the entire HSFS, and (2) characterize the gross morphology of fault scarps of this unusually broad fault system. Due to the width and complex geometry of the HSFS, profiling fault scarps using traditional methods (e.g., a stadia rod and abney level or even a total station) was not practical. Instead, we used a Trimble GEO XH GPS receiver with a Zephyr antenna to measure the location of points along the 15½- to 18½-km long profiles needed to transect the entire system. This GPS receiver employs real-time and post-processing differential corrections as well as filtering of erroneous reflections to greatly improve data precision beyond that of typical hand-held GPS receivers. With this GPS system, after post-processing the data using Pathfinder Office V4.0 and at least three different base stations in the Albuquerque region, accuracies are typically within 15 cm. For Profile P1, 90% of the data has estimated accuracies of 0 to 15 cm and 99% of the data has accuracies of 0 to 30 cm. For Profile P2, 94% of the data has accuracies of 0 to 15 cm, whereas 99.8% has accuracies of 0 to 30 cm. Due to time constraints and limited access in some areas, some of the transects were measured along dirt roads. In most cases this has only slightly modified the scarp morphology, but in a few cases grading of the road results in a more subdued scarp height and so estimated displacements measured along the road may be as much as ½ m less than displacements

measured across an undisturbed portion of the scarp. The limitations and uncertainties of the profiles are discussed further in Section 3.3, but regardless of these, the profiles and transects do provide a first-order approximation of cumulative displacements across the HSFS, and comparison of the relative scarp heights and morphologies for the different fault splays of the HSFS.

3.2 MAPPING RESULTS

Plate 1 shows the results of our mapping of Quaternary fault scarps on the Llano de Manzano surface between the Isleta Pueblo and the Sevilleta National Wildlife Refuge. Fault scarps were typically distinguished on the basis of linear breaks in slope that crosscut topography, offset or disrupt drainages and offset or warped surfaces. Some faults have an associated alignment of springs (e.g., splays J and L), which themselves have associated vegetation lineaments and light-colored spring deposits along portions of scarps. Some faults (usually those with larger scarps such as splays F, G, H, J, and L) partially expose buried soil carbonate horizons that form lighter colored lineaments, which subparallel scarp crests.

Based on our mapping, the HSFS is characterized by an unusually broad deformation zone of subparallel anastomozing normal faults that overall strike north-south and offset late Quaternary eolian and piedmont deposits down to the west a minimum of 28 to 41 m. Compared to previous mapping (c.f. Plate 1 with Figures 1 and 3), we have extended some fault traces farther south and added several new traces, resulting in a much longer total end-to-end, straight-line length of 73.5 km for the entire HSFS, compared to the previous total length of 43 km. The majority of the newly identified traces are located in the western half of the Llano de Manzano and the resulting width of the HSFS varies from a few to 18 km, but typically it is 10 to 14 km wide. We observed no evidence for any lateral component of slip along faults, although good piercing points to use as markers are generally lacking. In contrast, the Llano de Manzano surface is generally an excellent datum for identifying vertical offsets along fault scarps (e.g., Figures 6a and 6b). Despite the thick eolian cover on the Llano de Manzano, fault scarps are fairly continuous, except where they have been eroded by drainages and some short gaps due to complete burial by eolian sediments.

The wide, complex, anastomozing, and branching geometry of several subparallel faults make developing a consistent nomenclature for the HSFS challenging. For obvious reasons, we have abandoned the terms western, central, and eastern splays used by Maldonado et al. (1999; 2007) and Olig et al. (2007), except when we specifically refer to previous work. Instead, we have adopted the use of letters (A through Q on Plate 1) to refer to particular fault splays in our discussion of the HSFS. Even so, our nomenclature approach still has problems in tracing splays along strike due to branching, gaps, steps, and anastomozing geometries. For example, near profile P2 fault splay G branches to the north then merges with fault splay H (see top cover photograph), and then appears to make a small right step as it continues northward (Plate 1). Thus, although we refer to this fault as splay H on profile P1, alternatively we could have called it splay G or even splay G-H. Another example of the nomenclature complexity is splay J, which has one of the largest scarps across profile P1. Tracing this splay northward, it appears to connect to the same fault trenched by Personius and Mahan (2003) at the Hubbell Spring site (Plate 1), the western HSF. However, due to steps, gaps, and branching geometries, it is also

possible that the fault trenched at the Hubbell Spring site actually connects to a branch of fault splay L. Splay L was formerly referred to as the central HSF and was trenched to the south at the Carrizo Spring site by Olig et al. (2004) (Plate 1). This along-strike complexity of the HSFS not only complicates mapping and fault nomenclature, but more importantly poses a significant challenge for developing a complete paleoseismic record for the HSFS and understanding its rupture behavior. We discuss this further in Section 3.4.

In addition to its unusually broad and complex anastomozing geometry, the HSFS has some other unusual characteristics for normal faults, including a general lack of antithetic faults and backtilting in the hanging wall. There are a couple of antithetic faults within the HSFS (e.g., an antithetic fault to splay I north of profile P1, and an antithetic fault to splay H south of profile P2), but antithetic faults and backtilting in the hanging wall are unusually rare for the HSFS compared to typical normal faults.

In contrast, many faults of the HSFS show localized but prominent backtilting toward the east in the footwall. This unusual footwall backtilt is evident along many fault traces (shown by arrows on Plate 1) and sometimes results in long, linear closed-depressions and small playas that are surprisingly located on the upthrown side of scarps. The footwall backtilt also results in unusually broad scarps (as much as 2,200 m wide) with unusual morphologies that yield large uncertainties in estimating displacements. The unusual scarp morphologies and possible causes of the footwall backtilt are discussed in Section 3.3, but of particular relevance to the mapping are the large uncertainties in depicting these broad fault scarps depending on how they are mapped. For consistency, and to make our results as reproducible as possible, we show the crests of fault scarps as the location of fault traces on our map. We mapped the crests because they are the most distinctive and continuous features of the scarps. However, we point out that the actual fault planes are probably located somewhere between the crest and base of the scarps, and thus fault locations for the HSFS may have larger uncertainties than those of typical normal faults that have scarps that are only a few tens of meters wide.

V.S. Grauch (USGS, written communication, 2007) generously provided an updated interpretation of faults in the HSFS region based on aeromagnetic anomalies (revised and more detailed than Figure 3) to us for comparison with our mapping. Most of the splays that we mapped on the basis of fault scarps are associated with faults that she interpreted from aeromagnetic anomalies. Some notable exceptions are fault splays A through D that we mapped on the westernmost Llano de Manzano in the vicinity of Rio Communities and to the south (Plate 1). Although these fault scarps do not have associated aeromagnetic anomalies, they are prominent, long, and fairly continuous scarps. They show similar characteristics to the other fault scarps we mapped and we have no reason to believe that these scarps are not fault-related except for a couple of short, northeast and northwest-trending connecting scarps that are shown in lighter pink on Plate 1. These short suspect fault scarps subparallel drainages and may either be nontectonic or fault-related, but fluvially modified. Rawling (2004) also mapped fault scarps coincident with our splays D and G. He also shows buried faults inferred from aeromagnetic anomalies from Sweeney et al. (2002) coincident with our splays E, F, and H. Perhaps splays A through D are relatively new faults with cumulative displacements that are too small to show an associated aeromagnetic signature.

Another notable difference between mapped fault scarps and aeromagnetic faults is the general lack of late Quaternary fault scarps between fault splays J and L south of Meadow Lake (Plate 1), even though aeromagnetic anomalies are evident. We did observe very small (< 0.5 m) scarps in the road along profile P2, and in the road to the north (splays K? on Plate 1), but we could not trace these scarps farther north or south either in aerial photographs or in the field. A similar difference between mapped fault scarps and aeromagnetic faults exists for scarps associated with the southern end of splay L, which die out north of profile P2, whereas faults associated with aeromagnetic anomalies along splay L continue another 23 km southward, past Abo Arroyo. Perhaps late Quaternary movement on these buried faults has not kept pace with sedimentation rates in the area.

Although faults of the HSFS generally strike north-south and are down-to-the-west, south of where fault splay L dies out, traces trend more north-northeasterly and include a couple of long and prominent down-to-the-east fault scarps (i.e., splays P and Q on Plate 1). These scarps are 0.5 to 5 m high and 14 to 20 km long, do not appear antithetic to other faults, and do appear to align with faults interpreted from aeromagnetic anomalies (V.S. Grauch, written communication, 2007). These faults were previously mapped by Machette and McGimsey (1983), and referred to as unnamed faults on the Llano de Manzano (#2117 of Machette et al., 1998). They also are somewhat aligned with a northeast-trending gravity gradient in the southern Belen sub-basin (Grauch et al., 1999). However, the kinematic relation of these down-to-the-east faults to other faults of the HSFS is not clear, although based on their close proximity and similar geomorphic expression to other fault scarps of the HSFS, we do include them as part of the HSFS. Their more northeasterly trend also mimics the more northeasterly trend of the Los Piños Mountains range-front, which is about 5 to 10 km away. However, fault splays P and Q appear to show more late-Quaternary offset than the Los Piños fault, which apparently has no associated late Quaternary scarps (Machette et al., 1998). Thus, fault splays P and Q do not appear to be antithetic secondary faults of the Los Piños fault. Fault splays P and Q are 9 to 11 km south-southwest of the end of scarps associated with splay L, which is a major down-to-the-west fault. Although the buried Meadow Lake fault of Maldonado et al., 2007) may exhibit down to the east offset in the subsurface, it lies to the east of splay L and its aeromagnetic signature apparently does not extend south of 34°45’ (Tien Grauch, USGS, written communication, 2007). Furthermore, fault scarps associated with the eastern HSFS splay of Maldonado et al., (1999) north of Hells Canyon Wash are down to the west. We found no Quaternary fault scarps associated with the eastern HSFS splay of Maldonado et al., (1999) south of Hells Canyon Wash, which is over 39 km north of splays P and Q. In short, aside from splays P and Q, no other principal traces of the HSFS show evidence of down to the east displacement.

In Connell’s (2004) cross-section of the Belen sub-basin of the southern Albuquerque Basin, he shows east-dipping faults of the HSFS (coincident with splays P and Q), along with other west-dipping HSFS fault splays located to the west, as forming an axial horst and graben that serves as a hinge, accommodating rollover of Neogene strata in the hanging wall of an east-dipping low angle detachment fault. This detachment fault is at a depth of about 7 to 10 km in the vicinity of the HSFS and breaks the surface at the base of the Lucero uplift several tens of kilometers to the west of the HSFS. If this structural model is correct, hanging-wall style deformation may well explain the distributed and complex deformation patterns of the HSFS (including east-dipping faults P and Q), and overall westward dips of Neogene strata in the southern Belen sub-basin.

South of Abo Arroyo displacements are generally decreasing and there are fewer faults, with scarps of the HSFS appearing to die out just south of Black Butte on the southernmost Llano de Manzano (Plate 1). However, we acknowledge that our mapping may not be complete south of Highway 60. On the southwestern Llano de Manzano, drainages become more incised and the surface is much more dissected, particularly toward the Rio Grande. This dissection makes identifying faults scarps on aerial photographs more difficult and our field checking south of Abo Arroyo was limited due to time constraints. However, it is noteworthy that, except for the Contreras Cemetery fault mapped in the Abeytas Quadrangle by McCraw et al. (2006), Quaternary fault scarps were not identified in geologic mapping of the Abeytas, Becker, and La Joya 7.5' Quadrangles (McCraw et al., 2006; Luther et al., 2005; de Moor et al., 2005). The Contreras Cemetery fault is a northeast-striking, west-dipping normal fault that is approximately 5 km long (Plate 1; McCraw et al., 2006). It apparently does not extend southward into the La Joya Quadrangle (de Moor et al., 2005), but at its northern end it extends down off the western edge of the Llano de Manzano surface, offsetting a Rio Grande terrace (Qrgt3) by 2 to more than 4 m. This lowest terrace is estimated to be middle Pleistocene in age. (McCraw et al, 2006). We consider the Contreras Cemetery fault to be part of the HSFS based on its proximity, similar geometry, and kinematic compatibility with other faults of the southernmost HSFS.

Finally, we comment on the age of fault scarps shown on Plate 1. We did not conduct detailed mapping of all surficial deposits along the HSFS. However, most of the scarps appear to be offsetting eolian sands, alluvium, and colluvium that are inferred to be late Quaternary in age based on previous geologic mapping of the area (Karlstrom et al., 1999, 2000; Baer et al., 2004; Rawling, 2004; Rawling and McCraw, 2004; de Moor et al., 2005; Luther et al., 2005; Rawling, 2005; Scott et al., 2005; McCraw et al., 2006; and Maldonado et al., 1999, 2007), and previous trenching studies (Personius et al, 2001; Personius and Mahan, 2003; and Olig et al., 2004; 2005). Notable exceptions to this generality are the fault branches and traces located in the footwall of the southern end of splay L (Plate 1). These scarps are on early Pleistocene piedmont alluvium, Plio-Pleistocene Santa Fe Group sediments, and Triassic and Permian bedrock (Rawling and McCraw, 2004, Tome NE); therefore, these scarps could be much older than late Quaternary.

3.3 FAULT SCARP PROFILES

The locations of the two topographic profile transects, P1 and P2, are shown on Plate 1. The results of the topographic profile transects that we measured are shown both on Plate 1 (not vertically exaggerated), and on Figures 7 through 17 (vertically exaggerated as noted). Due to the broad and distributed nature of fault scarps, it was necessary to vertically exaggerate profiles to observe scarp morphologies and measure vertical surface displacements. Vertically exaggerated profiles were constructed using Grapher 3**.** Vertical surface offsets were calculated mathematically, using Grapher's line-fit capabilities, by determining the best linear fit for the hanging wall and footwall surfaces, and differencing the elevations at the mid-point of the scarp. Estimates of vertical surface displacements are shown in Table 2. The Llano de Manzano surface gently slopes 2° to 5° westward and is generally uniform, providing an excellent datum for measuring vertical displacements. However, as previously mentioned, several of the fault scarps exhibit localized backtilting in the footwall, which results in unusual scarp morphologies and large uncertainties in estimating displacements (e.g., Figures 7-9, 11-17).

The cause of the footwall backtilt along some HSFS splays is enigmatic. We know of no other example of such localized footwall backtilt that occurs so extensively on distributed normal faults. Surfaces locally dip as much as 7° to the east within backtilted zones. Typically footwall backtilting is localized along long narrow zones about 350 to 700 m wide, but ranges from 0 m (e.g., splay L; Figure 10) to over 1,000 m wide (e.g., splay G; Figure 15). Thus, although footwall backtilting related to isostatic rebound has been observed along some other normal faults (e.g., the Wasatch fault zone in Utah), that backtilt occurs on a crustal scale, across widths of tens of kilometers, and appears very different than the smaller-scale phenomenon observed on the HSFS. It is noteworthy that deposition of dune sand on the crests of some scarps has modified some scarp morphologies (e.g., splay D on P2; Figure 13) and perhaps even enhanced scarp heights. However, it is clear from the geometry and extent of the backtilted zones that they cannot be due to deposition alone. Additionally, backtilting on the HSFS does not appear to be dependent on scarp height as both small and large scarps show pronounced backtilting, whereas other small and large scarps show no backtilting. Similarly, backtilting does not appear to be associated only with scarps that have spring deposits or anastomozing geometries.

It is notable that the easternmost major fault, splay L, shows no footwall backtilt. This might suggest that backtilt is due to necessary space accommodation adjustments as HSFS faults to the west of splay L possibly change dip as they intersect and merge with splay L. However, this would not explain why many faults south of splay L show footwall backtilt, including fault splay P, which is backtilted to the west in the footwall of this down to the east scarp. It would also not explain why several faults to the west do not show footwall backtilt.

As previously discussed, Connell (2004) interprets a low angle detachment fault to exist under the western portion of the HSFS in the southern Belen sub-basin. Although this structural model may explain the distributed deformation patterns of the HSFS, and overall westward dips of Neogene strata in the southern Belen sub-basin, it would not explain the localized footwall backtilts to the east along the HSFS. Furthermore in his cross section, Connell (2004) also interprets the Manzano fault and a few additional west-dipping normal faults, as soling into a listric, west-dipping Montosa fault at depths of less than 5 km. The Montosa fault originally was a thrust fault that is exposed in the Manzano Mountains to the east, and is interpreted by Connell (2004) to have been reactivated as a normal fault during Neogene extension. If this structural model is correct, it raises the question of whether fault splay L of the HSFS also soles into the Manzano and Montosa faults, and whether footwall backtilts are somehow related to eastward rotation of overlying fault blocks. However, as splay L is one of the HSFS splays that does not show backtilting in the footwall, this does not appear to be a satisfactory explanation of backtilts either. As a side note, this structural model also raises the question of whether the Montosa fault is by inference an active seismogenic structure, even though there is no direct evidence for Quaternary offsets known along the Montosa fault.

In summary, although the scale and geometry of footwall backtilt along splays of the HSFS suggests it is related to secondary deformation, the cause of this unusual phenomenon and why it occurs on particular faults and not others remains enigmatic. If footwall backtilting is secondary, then it could be argued that displacement measurements should be made excluding backtilt. However, then some very large and continuous fault scarps would yield no measureable offset, which seems somewhat problematic. Additional studies, such as long trench excavations perhaps coupled with geophysical studies, are needed to better understand these backtilted zones

and why they formed on many splays of the HSFS so that they can be properly addressed in estimating displacements across the HSFS.

Pending a better understanding of the backtilted zones, in this study we estimate vertical surface displacements across the HSFS both excluding and including backtilts (minima and maxima, respectively, in Table 2). This results in large uncertainties in both vertical displacements and slip rates. For profile P1 the estimated cumulative vertical offsets across the entire HSFS range from 27.6 to 54.4 m, whereas for profile P2, the estimated cumulative vertical offset ranges from 41.4 to 83.1 m (Table 2).

We assumed ages of 80 to 130 ka to roughly estimate average late Quaternary vertical slip rates for the entire HSFS based on approximate ages of the oldest sediments predating faulting events exposed at the Carrizo Springs and Hubbell Springs trench sites (Olig *et al.*, 2004; Personius and Mahan, 2003). Using a maximum age of 130 ka and minimum displacements results in minimum cumulative vertical rates of 0.2 to 0.3 mm/yr for the HSFS. Using a minimum age of 80 ka and maximum offsets yields maximum cumulative vertical rates of 0.7 to 1.0 mm/yr. We emphasize that trenching of each fault splay across a transect of the entire HSFS is really needed to better determine rates both to reduce uncertainties in displacements (particularly due to the enigmatic nature of footwall backtilting) and ages. However, regardless of the large uncertainties, we believe these estimates are more representative of actual rates for the entire HSFS than previous estimates given the many previously unrecognized fault splays.

Displacements vary considerably along strike of individual fault splays of the HSFS and typically increase where splays merge. This, and the anastomozing geometry of traces suggests that there are complex patterns of slip transfer between fault splays of the HSFS, with northwest and northeast striking sections serving as relay ramps between principal north-south striking faults. Overall, the geometry and displacement patterns of the HSFS support treating all of these many fault traces as a fault system rather than as separate faults. Many more scarp profiles or other displacement measurements would be needed to better quantify these deformation patterns, but a sense of the along strike displacement variations is evident in the two scarp profile transects. Along transect P1 the largest displacements are across fault splays F, J and L. In contrast, to the south along transect P2, displacements are by far the largest on splay G, whereas displacements on splay L have completely died out (only lineaments remain), and displacements on splay J are much smaller and have almost died out (Table 2). Additional studies are definitely needed to better quantify the along-strike late Quaternary deformation patterns of the HSFS on the Llano de Manzano surface. Such studies would provide insight into potential rupture patterns and behavior of this complex fault system and may provide insights into the cause of footwall backtilts along many faults. Given the extensive nature of the Llano de Manzano surface and the HSFS, employing LiDAR would be an excellent tool for further investigating the deformation patterns of the HSFS.

3.4 SUMMARY AND DISCUSSION

Results from our Quaternary fault scarp mapping and profiling on the Llano de Manzano indicate that the HSFS is much longer, wider and more complex than previously thought and includes several newly discovered fault splays. It now is known to extend for about 74 km from the southern end of the Sandia Mountains to south of Black Butte and Abo Arroyo (Plate 1). It is

characterized by an unusually broad (as wide as 18 km, but typically 10 to 14 km wide and with 4 to 8 significant fault splays) deformation system of subparallel, anastomozing normal faults that overall strike north-south and offset late Quaternary eolian and piedmont deposits down to the west. Displacements vary considerably along strike of individual fault splays of the HSFS and typically increase where splays merge and decrease where they branch. These displacement variations, and the anastomozing geometry of fault traces suggests that there are complex patterns of slip transfer between fault splays of the HSFS, with northwest- and northeast-striking sections serving as relay ramps between principal north-south striking faults. Given the extensive nature of the HSFS and the Llano de Manzano surface, which provides an excellent datum for measuring vertical displacements, LiDAR would be a very useful tool for better quantifying the deformation patterns along the HSFS.

We only mapped Quaternary fault scarps between the Isleta Pueblo and the Sevilleta National Wildlife Refuge. However, we interpret the McCormick Ranch and Palace-Pipeline faults, which are previously mapped Quaternary faults in the Isleta Pueblo at the northern end of the HSFS (Love, 1996; Love et al., 1998; Maldonado et al., 1999; 2007), to be part of the HSFS based on their close proximity, similar anastomozing geometries and deformation patterns, and the along-strike projection and continuity of some fault traces between the HSFS and these faults. Based on similar arguments, we also consider the previously mapped Contreras Cemetery fault (McCraw et al., 2006) on the southernmost Llano de Manzano to be part of the HSFS.

Antithetic faults are rare in the HSFS, but several faults exhibit backtilting to the east within the footwall. This creates unusual scarp morphologies and results in large uncertainties in measuring vertical displacements. We measured scarp profiles along two long transects, P1 and P2, across the entire HSFS (Plate 1 and Figures 8 through 18). Vertical surface displacements measured on individual fault splays range from 0 to 31 m, whereas cumulative displacements for the HSFS range from 27.6 to 54.4 m across P1, and 41.4 to 83.1 m across P2 (Table 2). Estimating ages for the diachronous Llano de Manzano surface is somewhat problematic, but assuming all the offset occurred since 80-130 ka, based on ages from previous trench studies, yields vertical slip rates ranging from 0.2 to 0.7 mm/yr across P1, and from 0.3 to 1.0 mm/yr across P2. These rates are higher than previous estimates (even excluding backtilting, which increases estimated displacements) due to the increased number of faults and their subparallel, overlapping geometries.

The scale of the footwall backtilting (zones that are tens to hundreds of meters wide), and its pervasive distribution throughout the HSFS, suggests it is related to secondary deformation, but the ultimate cause of the footwall backtilting remains unknown. Several other faults in the Rio Grande rift exhibit similar fault trace patterns to the HSFS, with multiple subparallel anastomozing splays forming extensive normal fault systems (e.g., faults on the Llano de Albuquerque, the Jemez-San Ysidro fault zone, and the San Felipe fault zone); however, we know of no other faults that show pervasive backtilting in the footwall of scarps similar to the HSFS. Thus, additional studies of the HSFS, perhaps through a coupled program of trenching and geophysical investigations, is needed to better understand this unusual phenomenon and reduce uncertainties in estimated slip rates.

The longer, wider, and more complex faulting pattern of the HSFS raises structural questions about the subsurface geometry of the fault splays. Given the anastomozing geometry and close

proximity of some of the splays, it appears some merge at depth. However, given the west-dipping geometry of all but 2 splays, and the extensive length (up to 74 km) and width (up to 18 km) of the HSFS, it is also evident that all of the splays cannot merge together in the subsurface. This is also supported by interpretation of aeromagnetic anomalies, which indicates that several separate faults in the subsurface are distributed across the Llano de Manzano (Tien Grauch, USGS, written communication, 2007). Structural interpretations based on drill hole and other subsurface data also suggest several separate faults for the HSFS. In their cross section across the northern HSFS, Maldonado et al. (1999; 2007) show faults of the HSFS as separate, planar, moderately-dipping faults cutting Neogene strata tilted to the east. This is in sharp contrast to Connelll's (2007) interpretation of the southern HSFS, where faults cut west-dipping strata and are either in the hanging wall of a low-angle detachment to the west or sole into a listric normal fault to the east. Thus, despite apparent significant differences in structural style between the northern and southern portions, the HSFS likely includes several (at least 3, probably more) crustal-scale faults; however, additional study is obviously needed to better understand the subsurface geometry of the HSFS.

Most importantly to this study, the longer, wider more complex late Quaternary faulting pattern of HSFS has many implications for seismic hazards in the southern Albuquerque region. These include higher slip rates (0.2 to 1.0 mm/yr) as previously discussed, the potential for larger magnitude earthquakes, and the potential for much more complex rupture patterns with more earthquake sources affecting a much larger area. Additional paleoseismic studies are needed to better constrain slip rates and understand rupture patterns, displacements per event, recurrence intervals and paleomagnitudes.

The longer length of the HSFS is more consistent with the large displacements per event observed by Olig et al. (2004). However, the lack of any historical surface-ruptures with the length, width and complexity of the HSFS argues that the entire fault system probably does not typically rupture coseismically. Table 3 shows paleomagnitude estimates for the HSF using the empirical relations of Wells and Coppersmith (1994) based on surface-rupture length (L), and average (AD) or maximum (MD) along-strike displacement per event. Paleomagnitude estimates vary from M_w 6.6 to 7.5, depending on the rupture scenario and input parameter. Although more paleoseismic investigations are definitely needed to better understand rupture patterns and paleomagnitudes of the HSFS, it is also important to keep in mind that development of empirical relations used to estimate paleomagnitudes from lengths or displacements do not explicitly consider or account for zones of subparallel faults with multiple splays, such as the HSFS. These empirical relations may be totally inappropriate for multiple subparallel fault ruptures.

Given the multiple, overlapping, subparallel fault geometry of the HSFS, we believe that a comprehensive transect approach to future paleoseismic investigations of the HSFS is needed. This is in contrast to the more typical, but piecemeal, approach to selecting any suitable site along-strike. Thus, a group of geologically and logistically suitable sites in a transect perpendicular to, and across the entire fault system needs to be found. This obviously makes site selection more challenging than usual. The general location of the P1 transect may be a viable option as it has the advantages of: (1) geologically conducive sites along the transect; (2) good access along Monterey Bld..; (3) it is within the central portion of the system, but has a reasonable number of splays (probably 6, 7 at most); (4) one of the major faults, splay L, has

already been trenched near the transect; and, (5) options for undeveloped and accessible sites (outside of pueblos and wildlife/wilderness areas) look promising (although further research is needed regarding current landowners and gaining access/ permission). A comprehensive transect of trenches across faults along P1 would: (1) provide insights into the cause of backtilited zones and how to incorporate these into displacement estimates; (2) better constrain slip rates; and, (3) provide insights into the rupture behavior of individual splays to better understand rupture patterns, recurrence intervals and paleomagnitudes. Until these additional studies are done and the HSFS is better understood, it is probably best to model the HSFS in probabilistic hazard analyses as a zone of 4 to 8 parallel distributed faults that rupture randomly, with broad distributions of slip rates and maximum magnitudes to reflect the present large uncertainties as indicated in this study.

Table 2
Vertical Surface Displacements and Slip Rates Estimated From Scarp Profiles Measured Across the Hubbell Spring Fault System

Profile P1 – Monterey Boulevard:

	Fault Splay F	Fault Splay H	Fault Splay I[1]	Fault Splay J[1]	Fault Splay L[2]	Fault Splay M[2]	Fault Splay N[3]	Cumulative Across HSFS[4]	Estimated Average Late Quaternary Vertical Slip Rate (mm/yr)[5]
Minimum	11.3 m	1.9 m	0.8 m	4.0 m	7.2 m	2.4 m	0 m	27.6 m	0.2
Maximum (with backtilt in footwall)	16.0 m	9.0 m	2.2 m	16.0 m	Not applicable – no backtilt	4.0 m	0 m	54.4 m	0.7

Profile P2 – Capilla Peak:

	Fault Splay A	Fault Splay B	Fault Splay D	Fault Splay E	Fault Splay F[7]	Fault Splay G	Fault Splay H-I	Fault Splays J-K	Fault Splay L[3]	Fault Splay O[3]	Cumulative Across HSFS	Estimated Average Late Quaternary Vertical Slip Rate (mm/yr)[5]
Minimum	3.6 m	5.7 m[6]	5.0 m	Eroded	4.0 m	16.8 m	4.5 m	1.8 m	0 m	0 m	41.4 m	0.3
Maximum (with backtilt in footwall)	6.7 m	6.0 m	12.4 m	Eroded	14.0 m	31.2 m	9.0 m	3.8 m	0 m	0 m	83.1 m	1.0

1 For splays I and J combined the minimum and maximum estimates are 3.2 m and 19.0 m., respectively.

2 For splay L and M combined the minimum and maximum estimates are 11.2 m and 15.4 m, respectively.

3 Lineament only at the latitude of the profile transect.

4 For comparison, using combined splay results in cumulative minimum and maximum displacements of 27.6 m and 59.4 m, respectively.

5 Assuming an average age of 80 to 130 ka based partially on ages from Personius and Mahan (2003) and Olig et al. (2004; in review).

6 Estimate still includes some unknown amount of backtilt in footwall.

7 A drainage along the base of scarp may have enhanced apparent displacement along splay F.

Table 3

Paleomagnitude Estimates for Surface-Faulting Earthquakes on the HSFS

Fault Parameter[a]	Expected Moment Magnitude (M_w)[b]
L=74 km[c]	7.2
MD=4.7 m[d]	7.2
AD=1.7 m[e]	7.1
AD=4.7 m[f]	7.5
AD=0.4 m[g]	6.6
L=42 km[h]	7.0

[a] All surface rupture lengths (L) measured straight line, end to end. MD is maximum displacement and AD is minimum displacement per event.

[b] We used empirical relations from Wells and Coppersmith (1994) for all type of slip: Mw=5.08+1.16*log (L)σ, σ=0.28; Mw=6.93+0.82*log (AD), σ=0.39; Mw=6.69+0.74*log (MD), σ=0.04.

[c] For the entire HSFS and based on mapping in this study.

[d] Maximum observed displacement from Olig et al. (2004) for coseismic rupture of fault splays J and L; assumed to be representative of the maximum along-strike displacement of these splays.

[e] Minimum observed displacement of coseismic rupture of fault splays J and L from Olig et al. (2004); assumed to provide a lower bound of the average displacement for these splays.

[f] Maximum observed displacement for coseismic rupture of the western and central HSF; here assumed to provide an upper bound of AD of these splays.

[g] Preferred displacement for Event Y(?); applies to independent rupture of fault splay L only.

[h] For the rupture of splay L only and based on mapping in this study.

Baer, S., Karlstrom, K., Connell, S.D., 2004, Preliminary geologic map of the Manzano Peak 7.5-minute Quadrangle: New Mexico Bureau of Geology and Mineral Resources Draft Open-File Digital Geologic Map OF-GM 00, scale 1:24,000.

Chapin, C.E., 1971, The Rio Grande rift, Part I: Modifications and additions: New Mexico Geological Society, Guidebook 22, p. 191-201.

Chapin, C.E. and Cather, S.M., 1994, Tectonic setting of the axial basins of the northern and central Rio Grande rift: Geological Society of America Special Paper 291, p. 5-25.

Connell, S.D., Love, D.W., Sorrell, J.D., and Harrison, J.B.J, 2001, Plio-Pleistocene stratigraphy and geomorphology of the central part of the Albuquerque basin; 45th Field Conference of the Rock Mountain Cell of the Friends of the Pleistocene: New Mexico Bureau of Geology and Mineral Resources Open-File Report 454C and D, variously paginated.

Connell, S.D., 2004, Geology of the Albuquerque basin and tectonic development of the Rio Grande rift in north-central New Mexico, *in* Mack, G.H., and Giles, K.A., eds., The Geology of New Mexico, A Geologic History: New Mexico Geological Society, p. 359-388.

dePolo, C.M. and Slemmons, D.B., 1990, Estimation of earthquake size for seismic hazards: Geological Society of America Reviews in Engineering Geology, v. VIII, p. 1-27.

de Moor, M., Zinsser, A., Karlstrom, K., Chamberlin, R., Connell, S., and Read, A., 2005, Preliminary geologic map of the La Joya 7.5-minute Quadrangle: New Mexico Bureau of Geology and Mineral Resources, Draft Open-File Digital Geologic Map OF-GM 00, scale 1:24,000.

GRAM Inc. and William Lettis & Associates (WLA), 1995, Conceptual geologic model of the Sandia National Laboratories and Kirtland Air Force Base: Technical report to Sandia National laboratories, Albuquerque, New Mexico, December 1995, various pagination.

Grauch, V.J.S., 1999, Discussion of new gravity maps for the Albuquerque basin area, *in* Pazzaglia, F.J., and Lucas, S.G., eds., Albuquerque geology: New Mexico Geological Society Guidebook, v. 50, p. 119-124.

Grauch, V.J.S., 2001, High-resolution aeromagnetic data, a new tool for mapping intrabasinal faults: Example from the Albuquerque basin, New Mexico: Geology, v. 29, no. 4, p. 367-370.

Grauch, V.J.S. and Hudson, M.R., 2002, Implications of significant distances between major faults and large vertical displacements based on geophysical evidence, central Rio Grande rift, New Mexico: Geological Society of America Abstracts with Programs, v. 34, no. 6, p. 452.

Hawley, J.W., 1986, Physiographic provinces (and) landforms of New Mexico *in* Williams, J.L., ed., New Mexico in Maps: Albuquerque, The University of New Mexico Press, p. 28-31.

Hawley, J.W., Haase, C.S., and Lozinsky, R.P., 1995, An underground view of the Albuquerque basin; *in* Ortega-Klett, C.T., ed., The water future of Albuquerque and the middle Rio Grande basin: New Mexico Water Resources Research Institute, p. 27-55.

Hawley, J.W., Kottlowski, F.E., Seager, W.R., King, W.E., Strain, W.S., and LeMone, D.V., 1969, The Santa Fe Group in the south-central New Mexico border region: New Mexico Bureau of Mines and Mineral Resources, Circular 104, p. 235-274.

Hudson, M.R. and Grauch, V.J.S., 2003, Paleomagnetic evidence for a Tertiary not Triassic age for rocks in the lower part of the Grober-Fuqua #1 well, southeastern Albuquerque basin, New Mexico: New Mexico Bureau of Geology and Mineral Resources, New Mexico Geology, v. 25, no. 2, p. 31-36.

Karlstrom, K., Connell, S.D., Rodgers, S.A., and Crawford, E.B., 2000, Preliminary geologic map of the Capilla Peak 7.5-minute Quadrangle: New Mexico Bureau of Geology and Mineral Resources Draft Open-File Digital Geologic Map OF-GM 00, scale 1:24,000.

Karlstrom, K., Connell, S.D., Rodgers, S.A., and Crawford, E.B., 1999, Preliminary geologic map of the Bosque Peak Quadrangle, Valencia, Torrance, and Bernalillo Counties, New Mexico: New Mexico Bureau of Geology and Mineral Resources Draft Open-File Digital Geologic Map OF-GM 24, scale 1:24,000.

Keller, G.R. and Cather, S.M., editors, 1994, Basins of the Rio Grande rift: Structure, stratigraphy, and tectonic setting: Geological Society of America Special Paper 291, 304 p.

Kelley, V.C., 1977, Geology of Albuquerque Basin, New Mexico: New Mexico Bureau of Mines and Mineral Resources, Memoir 33, 59 pp.

Love, D.W., 1998, Geology of the Isleta 7.5-minute quadrangle, Bernalillo and Valencia Counties, New Mexico: New Mexico Bureau of Mines and Mineral Resources, Open-File Digital Map DM 13, scale 1:24,000.

Love, D.W., Hitchcock, C., Thomas, E., Kelson, K., Van Hart, D., Cather, S., Chamberlin, R., Anderson, O., Hawley, J., Gillentine, J., White, W., Noler, J., Sawyer, T., Nyman, M., and Harrison, B., 1996, Geology of the Hubbell Spring 7.5-min quadrangle, Bernalillo and Valencia Counties, New Mexico: New Mexico Bureau of Mines and Mineral Resources Open-File Digital Geologic Map 5, scale 1:12,000.

Lozinsky, R.P., 1994, Cenozoic stratigraphy, sandstone petrology, and depositional history of the Albuquerque Basin, central New Mexico: Geological Society of America Special Paper 291, p. 73-81.

Luther, A. L., Karlstrom, K., Scott, L.A.,Elrick, M., and Connell, S.D., 2005, Preliminary geologic map of the Becker 7.5-minute Quadrangle: New Mexico Bureau of Geology and Mineral Resources Draft Open-File Digital Geologic Map OF-GM 100, scale 1:24,000.

Machette, M.N., 1978, Geologic map of the San Acacia quadrangle, Socorro County, New Mexico: U.S. Geological Survey, Geologic Quadrangle Map GQ-1415, scale 1:24,000.

Machette, M.N., 1982, Quaternary and Pliocene faults in the La Jencia and southern part of the Albuquerque-Belen basins, New Mexico: Evidence of fault history from fault-scarp morphology and Quaternary geology, New Mexico Geological Society Guidebook, 33rd Field Conference, p. 161-169.

Machette, M.N., 1985, Calcic soils of the southwestern United States, *in* Weide, D.L., ed., Quaternary soils and geomorphology of the American Southwest: Geological Society of America Special Paper 203, p. 1-21.

Machette, M.N. and McGimsey, R.G., 1983, Map of Quaternary and Pliocene faults in the Socorro and western part of the Fort Sumner 1º x 2º quadrangles, central New Mexico: U.S. Geological Survey, Miscellaneous Field Studies, Map MF-1465-A, scale 1:250,000.

Machette, M.N., Personius, S.F., Kelson, K.I, Haller, K.M., and Dart, R.L., 1998, Map and data for Quaternary faults and folds in New Mexico: U.S. Geological Survey, Open-File Report 98-521, 443 p.

Maldonado, F., Connell, S.D., Love, D.W., Grauch, V.J.S., Slate, J.L., McIntosh, W.C., Jackson, P.B., and Byers, F.M., Jr., 1999, Neogene geology of the Isleta Reservation and vicinity, Albuquerque basin, New Mexico, *in* Pazzaglia, F.J., and Lucas, S.G., eds., Albuquerque geology: New Mexico Geological Society Guidebook, v. 50, p. 175-188.

Maldonado, F., Slate, J.L., Love, D.W., Connell, S.D., Cole, J.C., and Karlstrom, K.E., 2007, Geologic map of the Pueble Isleta Tribal Lands and Vicinity, Bernalillo, Torrance, and Valencia Counties, Central New Mexico: U.S. Geological Survey Scientific Investigations Map 2913.

McCalpin, J.P., 1995, Frequency distribution of geologically determined slip rates for normal faults in the western U.S.: Bulletin of the Seismological Society of America, v. 85, p. 1867-1872.

McCalpin, J.P., Olig, S.S., Harrison, J.B.J., and Berger, G.W., 2006, Quaternary faulting and soil formation on the County Dump fault, Albuquerque, New Mexico: New Mexico Bureau of Geology and Mineral Resources Circular 212, 36 p.

McGraw, D.J., Love, D.W., and Connell, S.D., 2006, Preliminary geologic map of the Abeytas Quadrangle, Socorro County, New Mexico: New Mexico Bureau of Geology and Mineral Resources, Open-File Digital Geologic Map OF-GM 121, scale 1:24,000.

Morgan, P., Seager, W.R., and Golombek, M.P., 1986, Cenozoic thermal, mechanical and tectonic evolution of the Rio Grande rift: Journal of Geophysical Research, v. 91, p. 6263-6276.

Olig, S.S. Eppes, M.C., Forman, S. L., Love, D.W., and Allen, B.D., in review, Late Quaternary earthquakes on the Hubbell Spring fault system, New Mexico, USA: Evidence for complex non-characteristic ruptures of intrabasin faults in the Rio Grande rift, Geological Society of America Special Paper.

Olig, S.S. Eppes, M.C., Forman, S. L., Love, D.W., and Allen, B.D., 2004, Paleoseismic investigation of the central Hubbell Spring fault, central New Mexico: URS Corporation unpublished Final Technical Report to the U.S. Geological Survey, NEHRP Award No. 99HQGR0089, URS Job No. 26813901, variously paginated.

Olig, S.S. Eppes, M.C., Forman, S. L., Love, D.W., and Allen, B.D., 2005, Prehistoric earthquakes on the Hubbell Spring fault: Evidence for coseismic noncharacteristic rupture of intrabasin faults in the Rio Grande rift, *in* Proceedings Volume of the Basin and Range Province Seismic Hazards Summit II, Lund, W.R., (ed.), Utah Geological Survey Miscellaneous Publication 05-2, p. 114-117 (variously paginated).

Olig, S., Zachariasen, J. Wong, I.G., and Dober, M.C., 2007, Paleoseismic evidence for longer and more complex rupture patterns on the Hubbell Spring fault system, Rio Grande rift, New Mexico: Implications for recurrence models and their use in hazard analysis (abs.), Seismological Research Letters, v. 78, No. 2 p. 315.

Personius, S.F., Eppes, M.C., Mahan, S.A., Love, D.W., Mitchell, D.K., and Murphy, A., 2001, Log and data from a trench across the Hubbell Spring fault zone, Bernalillo County, New Mexico: U.S. Geological Survey Miscellaneous Field Studies Map MF-2348, v. 1.1.

Personius, S.F., Machette, M.N., and Kelson, K.I, 1999, Quaternary faults in the Albuquerque area – An update, in Pazzaglia, F.J., and Lucas, S.G., eds., Albuquerque Geology: New Mexico Geological Society Guidebook, v. 50, p. 189-200.

Personius, S.F. and Mahan, S.A., 2003, Paleoearthquakes and eolian-dominated fault sedimentation along the Hubbell Spring fault zone near Albuquerque, New Mexico: Bulletin of the Seismological Society of America, v. 93, no. 3, p. 1,355-1,369.

Rawling, G., 2004, Preliminary geologic map of the Tome 7.5-minute Quadrangle: New Mexico Bureau of Geology and Mineral Resources Draft Open-File Digital Geologic Map OF-GM 90, scale 1:24,000.

Rawling, G., 2005, Preliminary geologic map of the Tome SE 7.5-minute Quadrangle: New Mexico Bureau of Geology and Mineral Resources Open-File Digital Geologic Map OF-GM 109, scale 1:24,000.

Rawling, G., and McCraw, D.J., 2004, Preliminary geologic map of the Tome NE 7.5-minute Quadrangle: New Mexico Bureau of Geology and Mineral Resources Draft Open-File Digital Geologic Map OF-GM 00, scale 1:24,000.

Read, C.B., Wilpolt, R.H., Andrews, D.A., Summerson, C.H., and Wood, G.H., 1944, Geologic map and stratigraphic sections of Permian and Pennsylvanian rocks of parts of San Miguel, Santa Fe, Sandoval, Bernalillo, Torrance, and Valencia Counties, north-central New Mexico: U.S. Geological Survey Oil and Gas Investigations Preliminary Map 21, 1 sheet, scale 1:190,080.

Reiche, P., 1949, Geology of the Manzanita and North Manzano Mountains, New Mexico: Geological Society of America Bulletin, v. 60, p. 1183-1212.

Russell, L.R. and Snelson, S., 1994, Structure and tectonics of the Albuquerque Basin segment of the Rio Grande rift: Insights from reflection seismic data: Geological Society of America Special Paper 291, p. 82-112.

Sanford, A.R., Jaksha, L.H., and Cash, D.J., 1991, Seismicity of the Rio Grande rift in New Mexico, in D.B. Slemmons, E.R. Engdahl, M.D. Zoback, and D.D. Blackwell (eds), Neotectonics of North America, Geological Society of America Decade Map, v. 1, p. 229-244.

Scott, L.A., Elrick, M., Connell, S.D., and Karlstrom, K., 2005, Preliminary geologic map of the Scholle 7.5-minute Quadrangle: New Mexico Bureau of Geology and Mineral Resources Draft Open-File Digital Geologic Map OF-GM 99, scale 1:24,000.

Stark, J.T., 1956, Geology of the south Mazano Mountains, New Mexico: New Mexico Institute of Mining and Technology, State Bureau of Mines and Mineral Resources Bulleting 34, 49 p.

Sweeney, R.E., Grauch, V.J.S., and Phillips, J.D., 2002, Merged digital aeromagnetic data for the Middle Rio Grand and Southern Espanola Basins, New Mexico: U.S. Geological Survey Open-File Report 02-205, 17 p.

Titus, F.B., Jr., 1963, Geology and ground-water conditions in eastern Valencia County, New Mexico: New Mexico Bureau of Mines and Mineral Resources Ground-Water Report 7, 113 p., 2 pls., scale 1:125,000.

Wells, D. L. and Coppersmith, K. J., 1994, Analysis of empirical relationships among magnitude, rupture length, rupture area, and surface displacement: Bulletin of the Seismological Society of America, v. 84, p. 974-1002.

Wong I., Olig, S., Dober, M., Silva, W., Wright, D., Thomas, P., Gregor, N., Sanford, A., Lin, K.W., Love, D., and Naugler, W., 2000, A new generation of earthquake ground shaking hazard maps for three urban areas in the western U.S.: Part II Albuquerque-Belen-Santa Fe, New Mexico corridor, in Proceedings, Sixth International Conference on Seismic Zonation, v. I, p. 369-374.

Woodward, L.A., 1982, Tectonic framework of Albuquerque County: New Mexico Geological Society, Guidebook 33, p. 141-146.

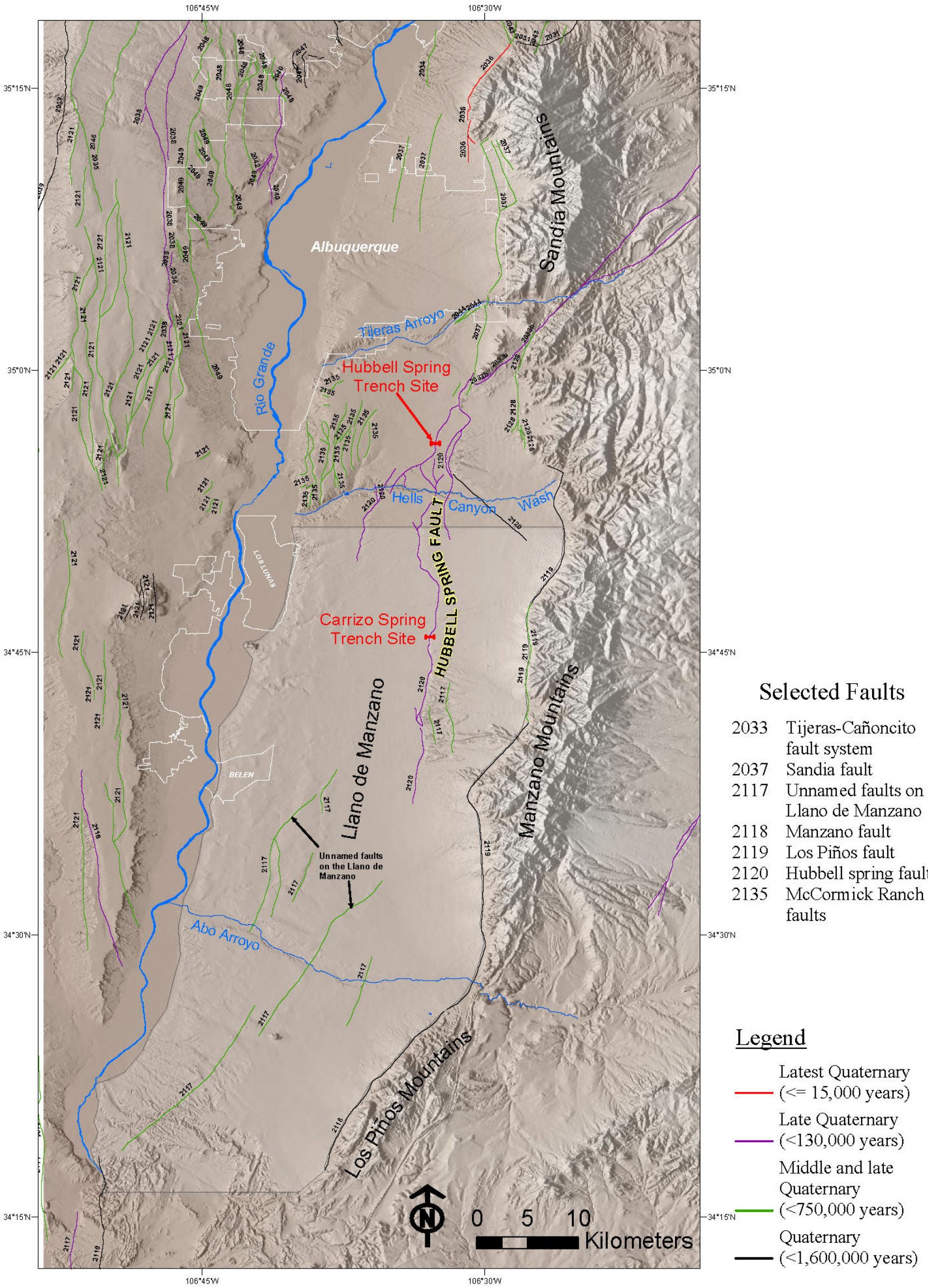

Figure 1. Previously mapped Quaternary faults in the southern Albuquerque area (modified from Machette et al., 1998). Fault identification numbers are the same as those used in the USGS Quaternary Fault and Fold Database (http://qfaults.cr.usgs.gov). Compare outlined area with our mapping for this study on Plate 1.

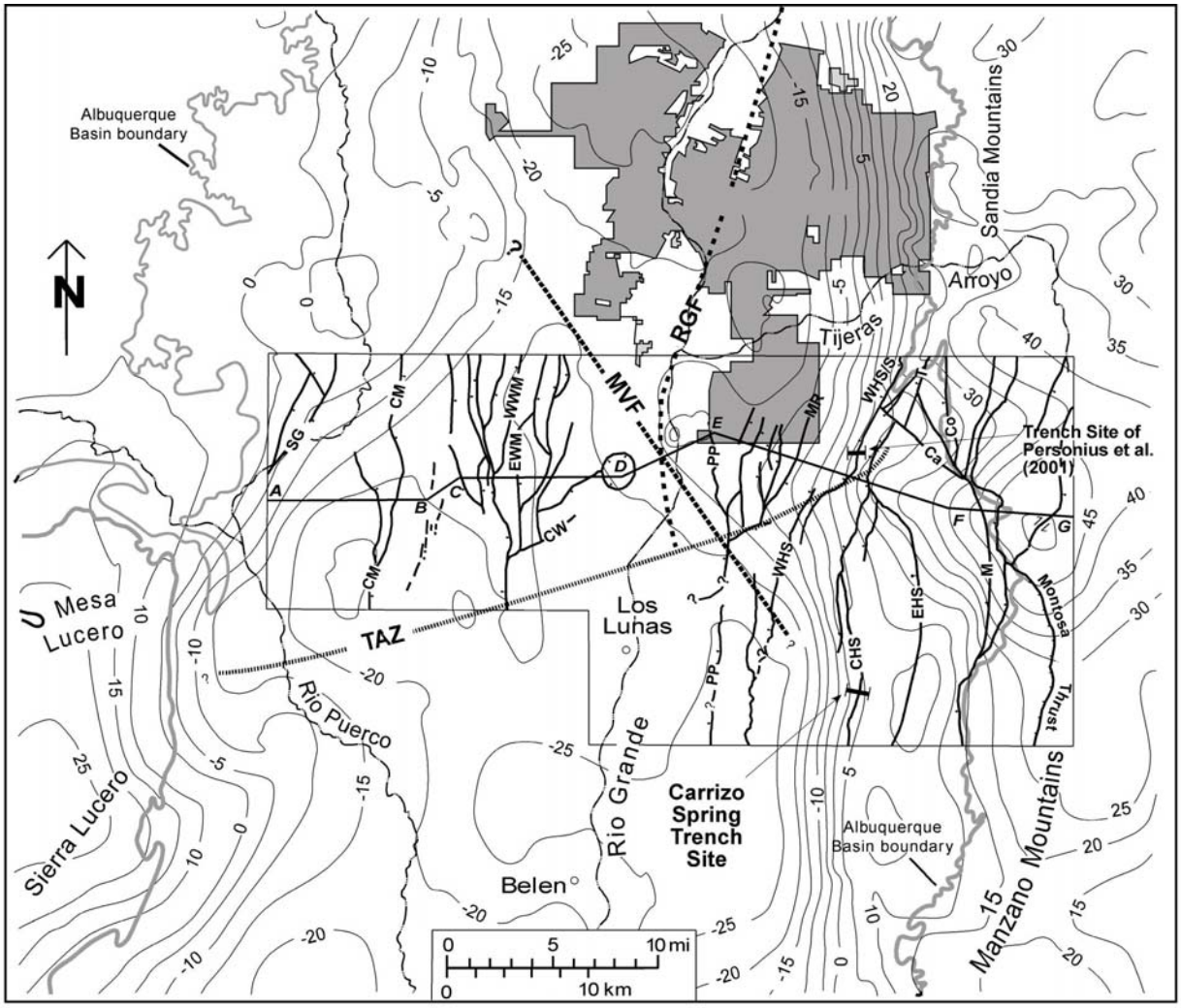

Figure 2. Isostatic residual gravity anomaly map (5 mgal contours) superimposed on the northern **Hubbell Spring fault system (HSFS)** (modified from Maldonado *et al*., (1999). Line of cross-section A through G is keyed to their Figure 4. Abbreviation key: Ca-Colorado fault, **CHS-Central Hubbell Spring fault**, Co-Coyote fault, CM- Cat Mesa fault, CW-Cedar Wash fault, **EHS-Eastern Hubbell Spring fault**, EWM Eastern Wind Mesa fault, M-Manzano fault, **MR-McCormick Ranch faults**, MVF-inferred Mountain View fault, **PP-Palace-Pipeline fault**, S-Southern Sandia fault, SG South Garcia fault, T-Tijeras fault, TAZ-inferred Tijeras accommodation zone, **WHS-Western Hubbell Spring fault**, and WWM-Western Wind Mesa fault

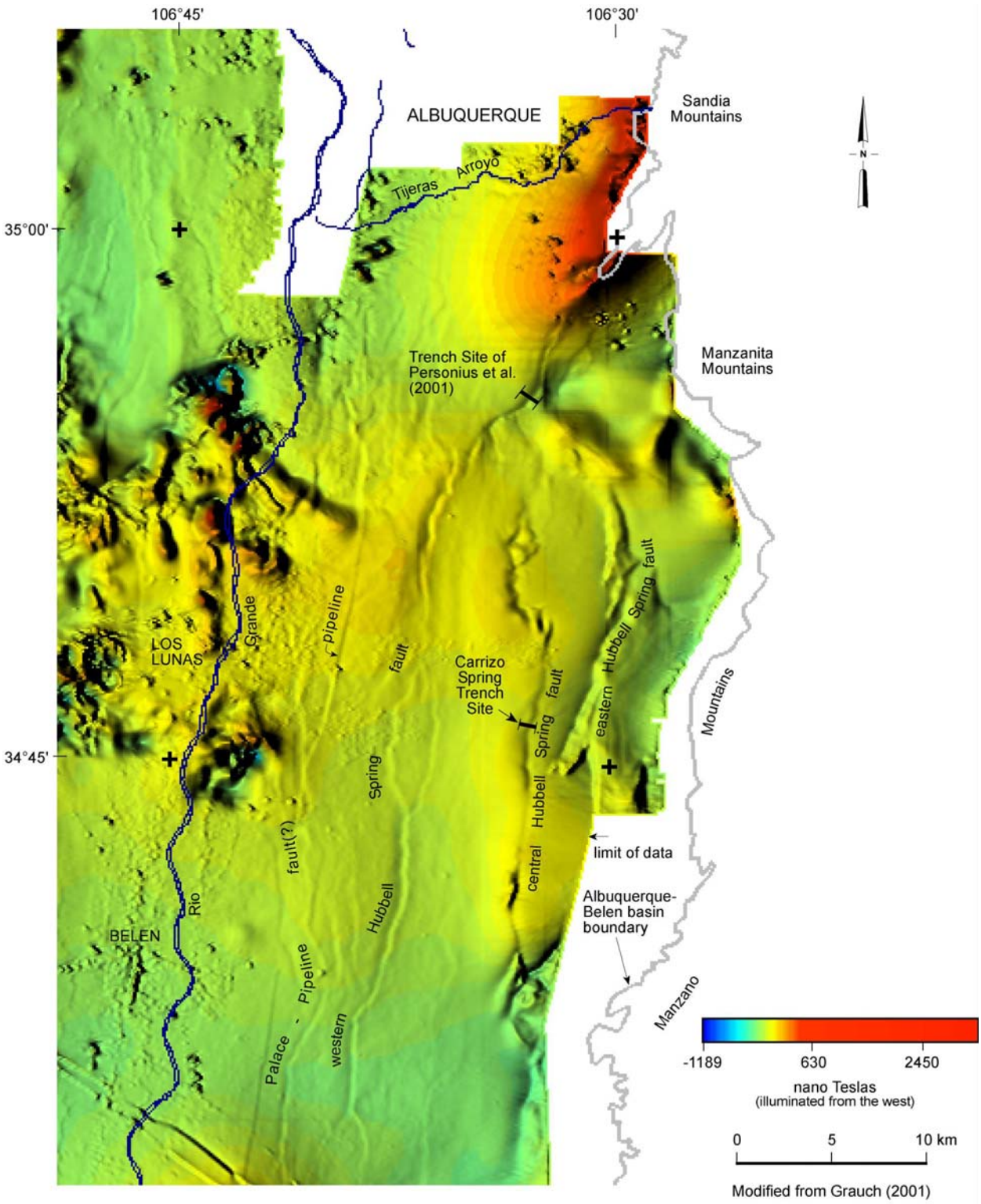

Figure 3. Color shaded-relief aeromagnetic image of the Hubbell Spring fault system, illuminated from the west (modified from Grauch, 2001). Fault nomenclature follows that of Maldonado *et al.* (1999).

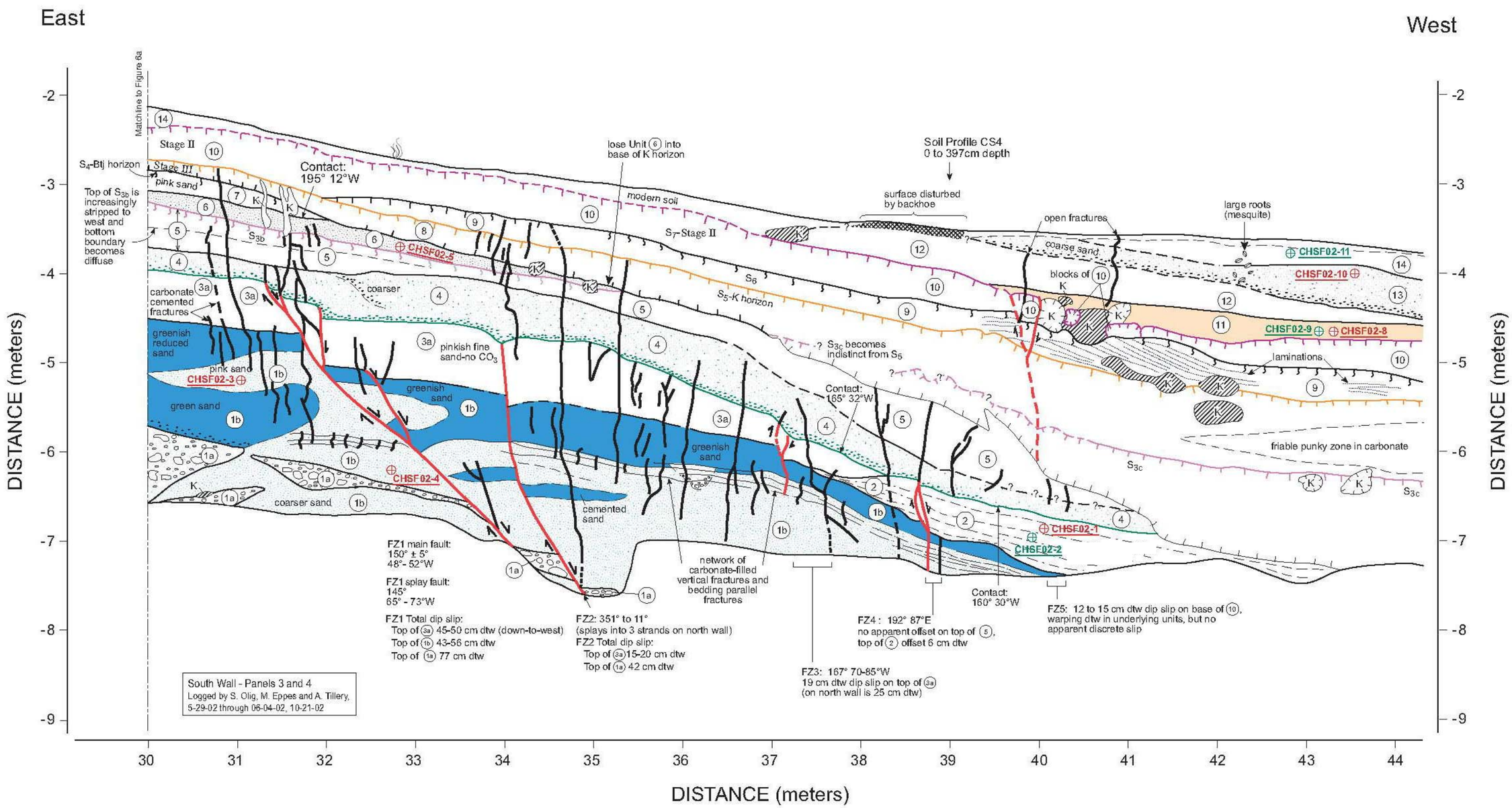

Figure 4. Portion of the Carrizo Spring trench log (Olig *et al.*, 2004) showing locations of additional luminescence samples (in green) analyzed for this study (CHSF02-2, CHSF02-9, and CHSF02-11). See Olig *et al.* (2004; in review) for unit descriptions and detailed discussion of paleoseismic events.

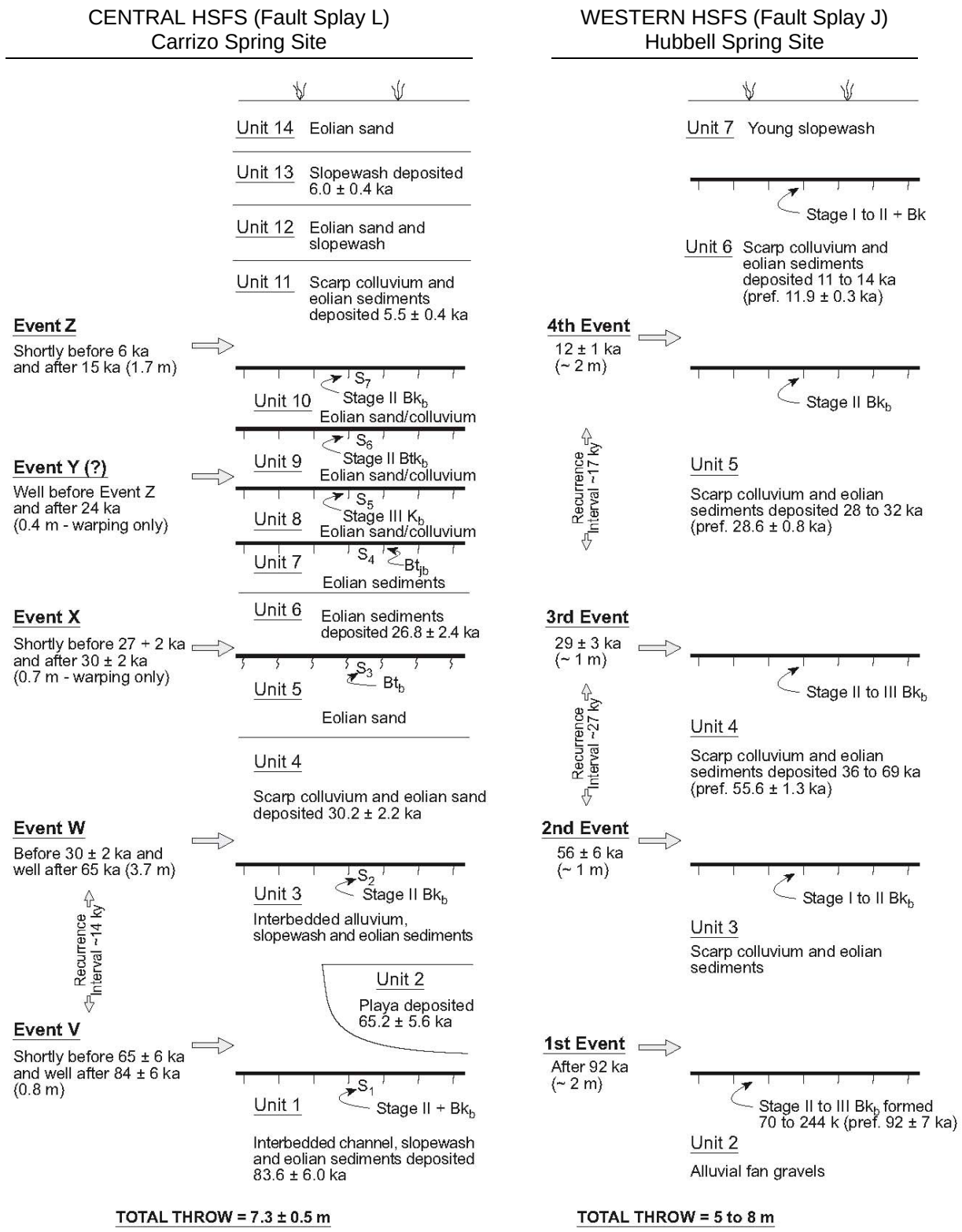

Figure 5. Comparison of the paleoseismic records of the central (Olig et al., 2004) and western (Personius and Mahan, 2003) splays of the HSFS (from Olig et al., in review).

(a)

(b)

Figure 6. Photographs looking west along Monterey Blvd. (and profile P1) at fault scarps of: (a) splay J (see Figure 9 for profile), and (b) splay L (see Figure 10 for profile). Bosque Peak is visible in the background of both photographs.

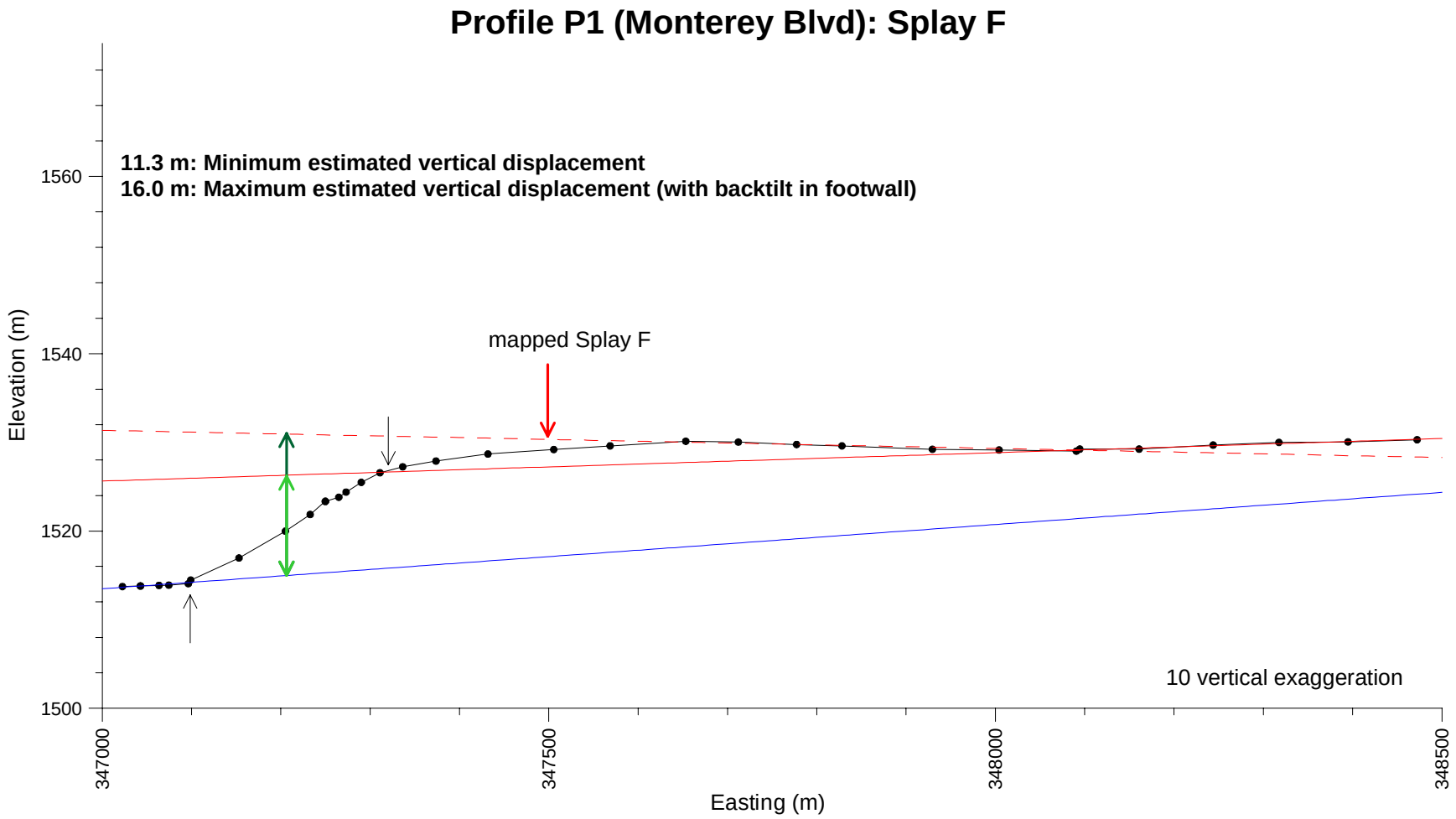

Figure 7. Vertically exaggerated section of Topographic Profile P1 at Fault Splay F. Estimates of net vertical surface displacements were measured midway between scarp crest and base (shown by gray arrows) at location of double-headed green arrows.

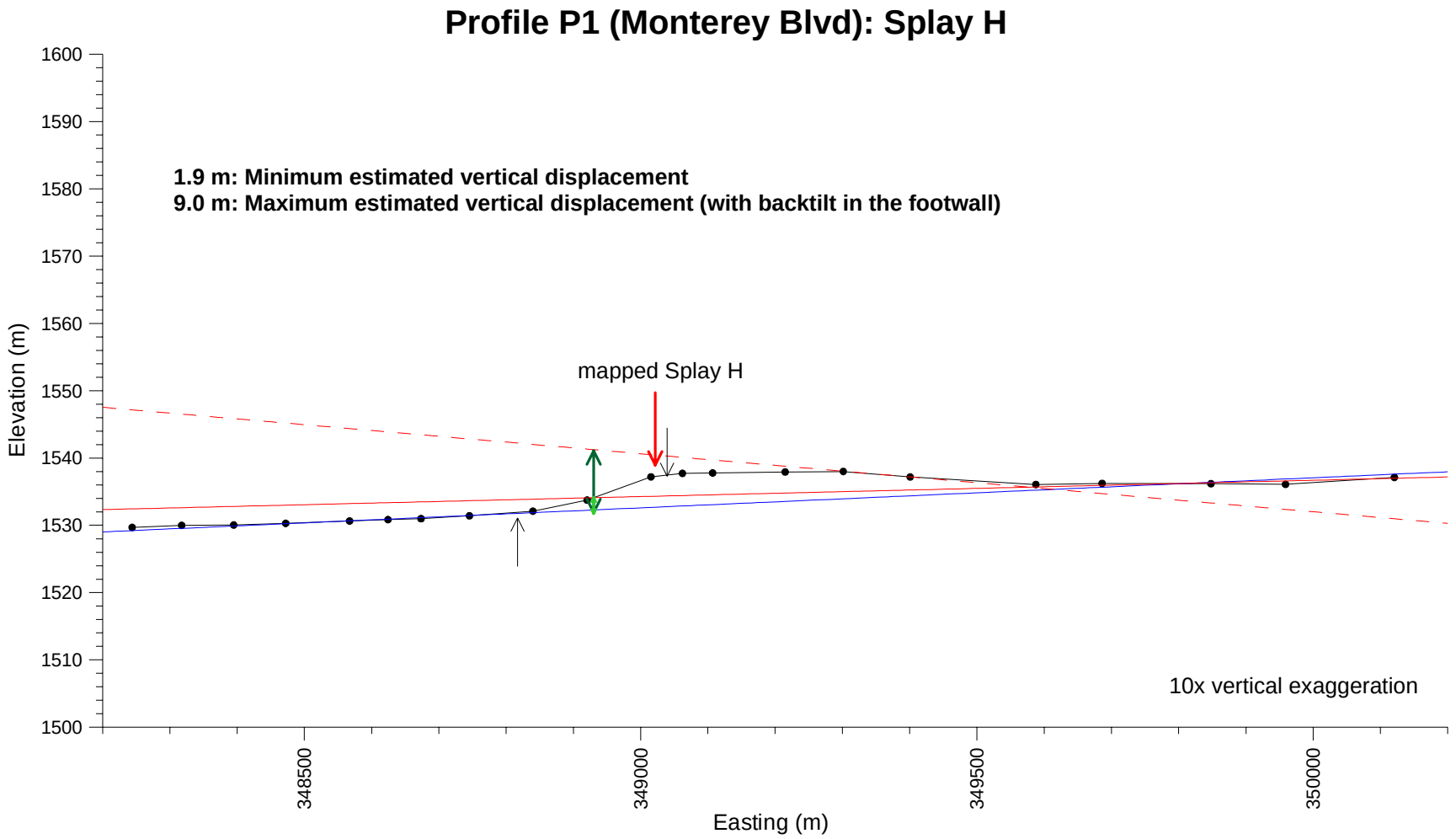

Figure 8. Vertically exaggerated section of Topographic Profile P1 at Fault Splay H. Estimates of net vertical surface displacements were measured midway between scarp crest and base (shown by gray arrows) at location of double-headed green arrows.

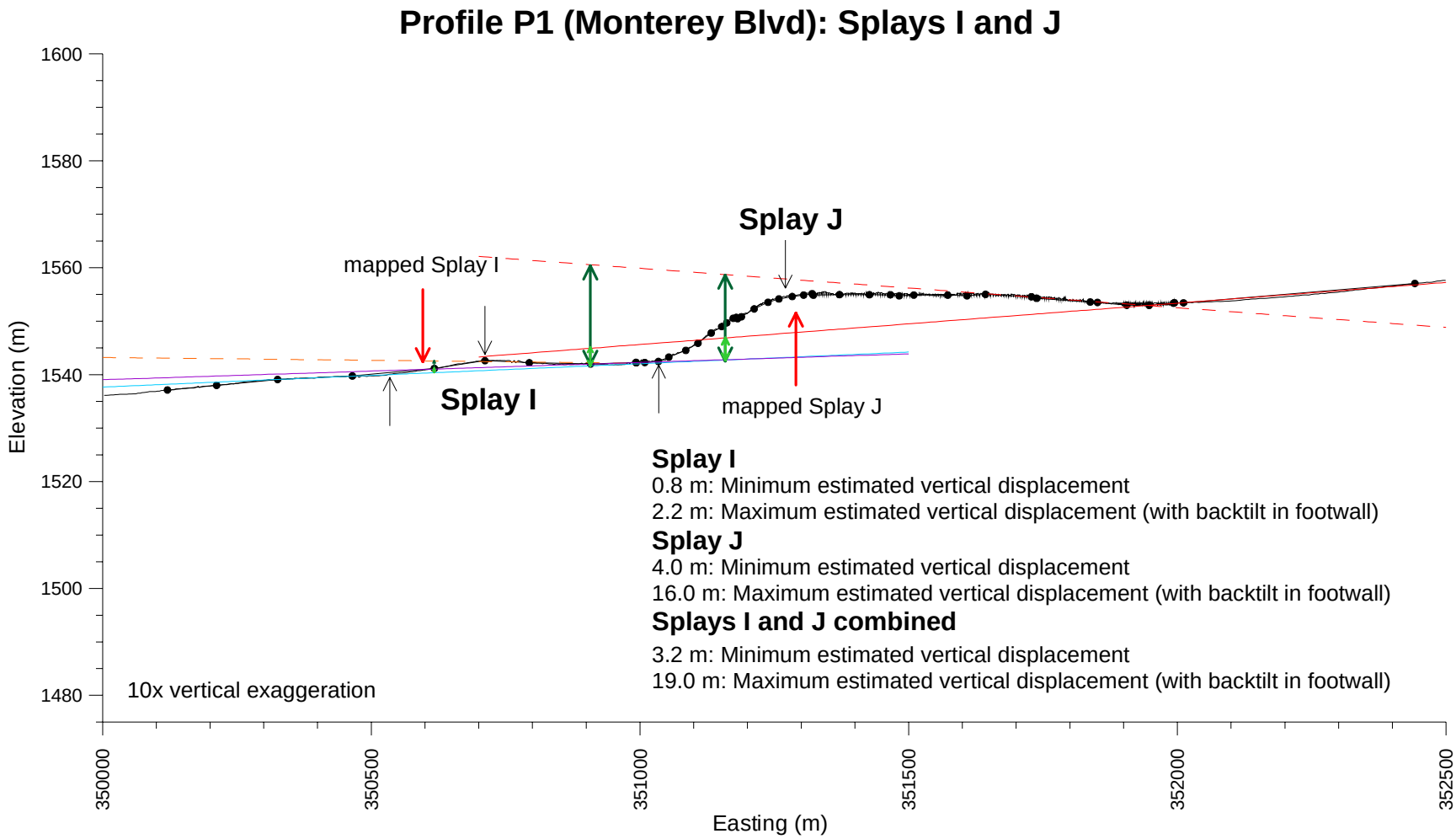

Figure 9. Vertically exaggerated section of Topographic Profile P1 at Fault Splays I and J. Estimates of net vertical surface displacements were measured midway between scarp crest and base (shown by gray arrows) at location of double-headed green arrows.

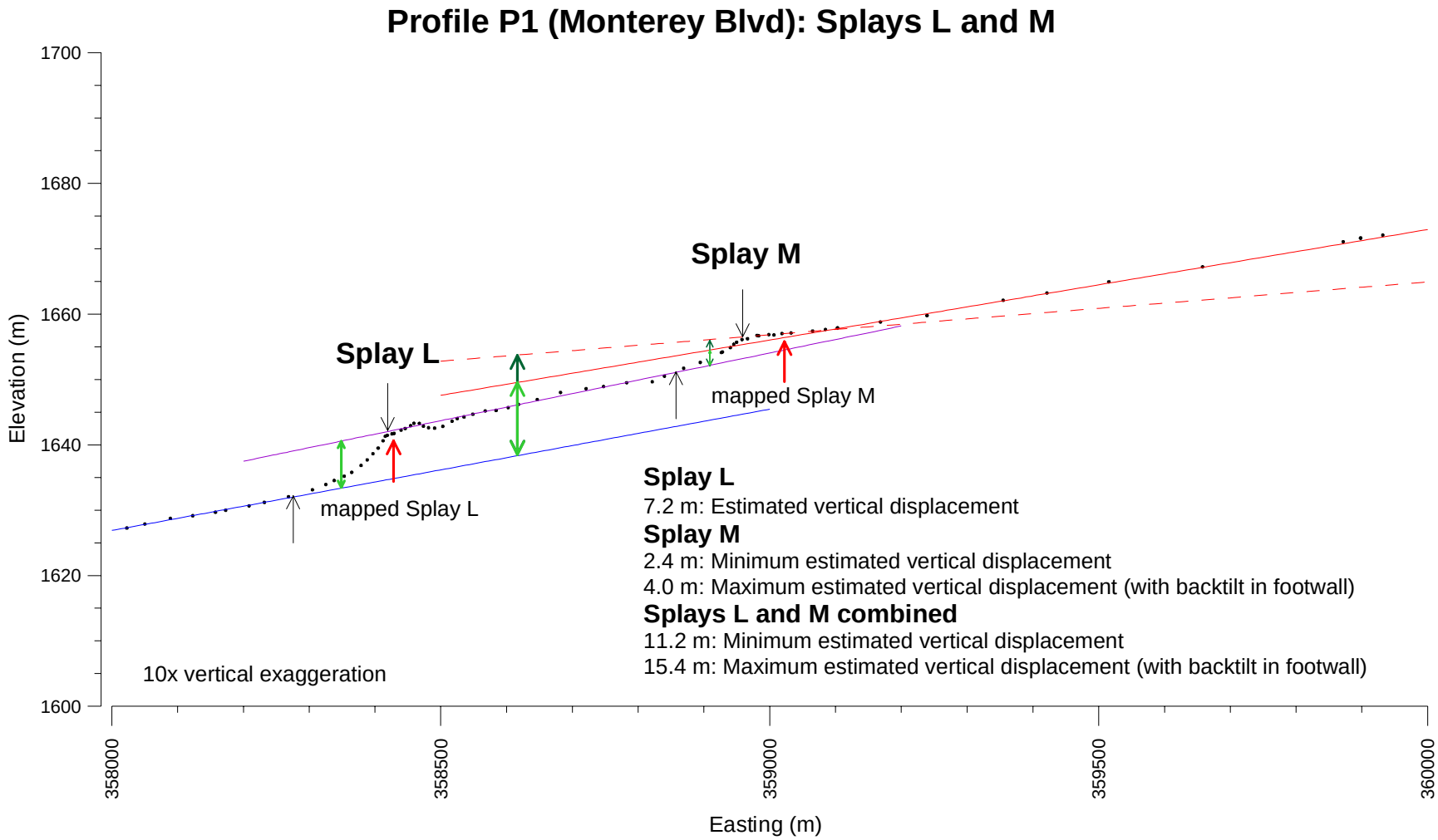

Figure 10. Vertically exaggerated section of Topographic Profile P1 at Fault Splays L and M. Estimates of net vertical surface displacements were measured midway between scarp crest and base (shown by gray arrows) at location of double-headed green arrows.

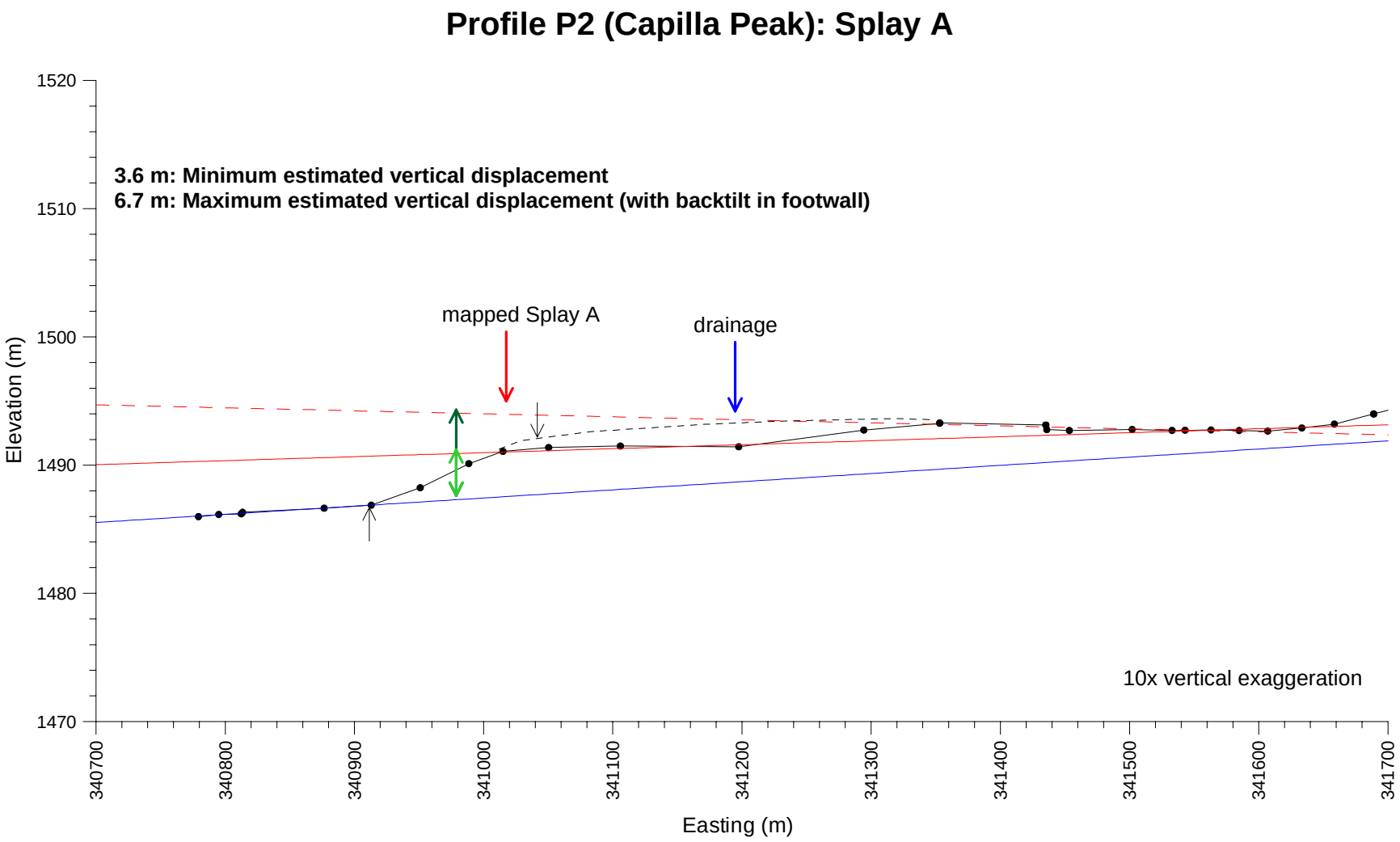

Figure 11. Vertically exaggerated section of Topographic Profile P2 at Fault Splay A. Estimates of net vertical surface displacements were measured midway between scarp crest and base (shown by gray arrows) at location of double-headed green arrows.

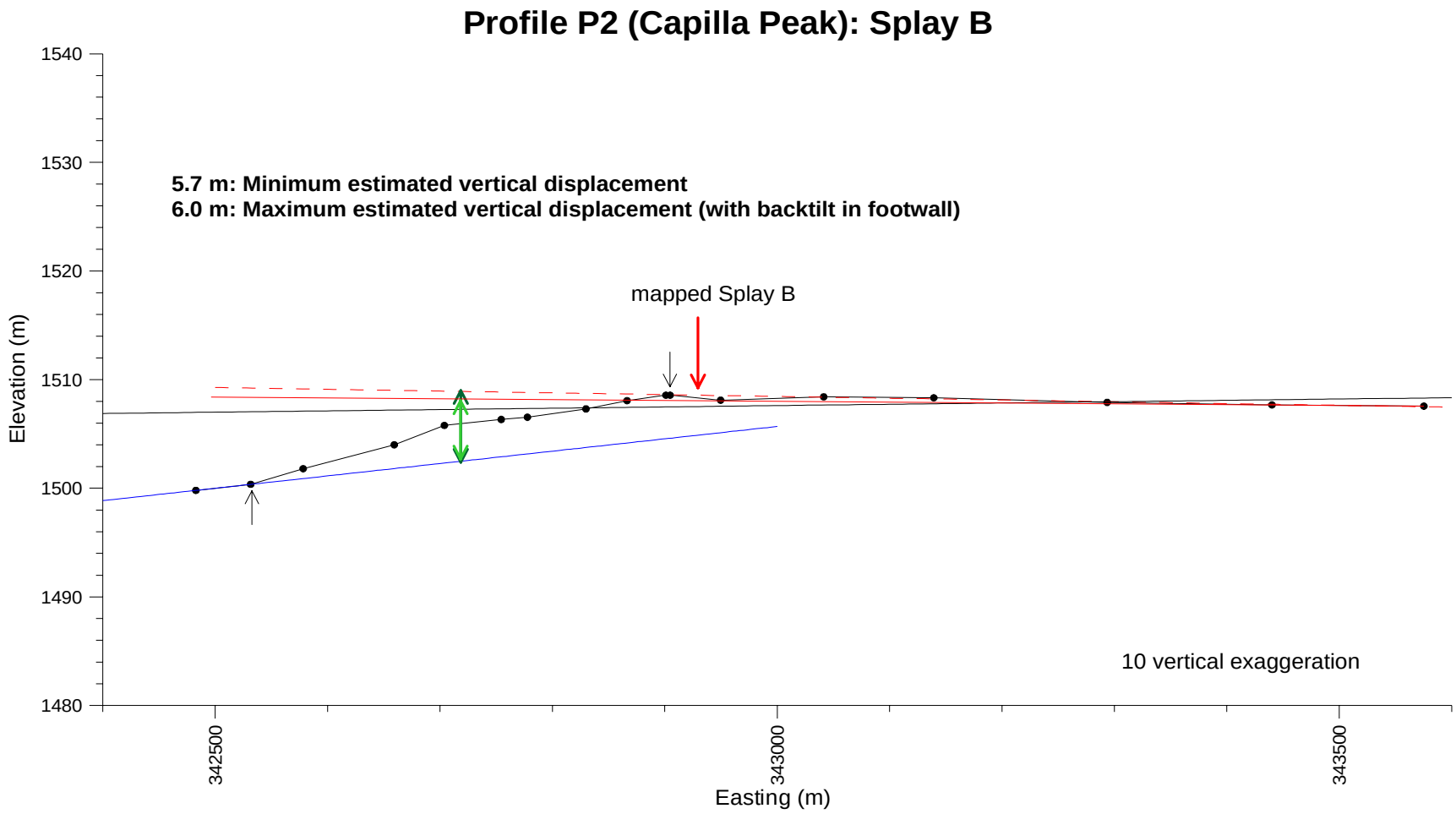

Figure 12. Vertically exaggerated section of Topographic Profile P2 at Fault Splay B. Estimates of net vertical surface displacements were measured midway between scarp crest and base (shown by gray arrows) at location of double-headed green arrows.

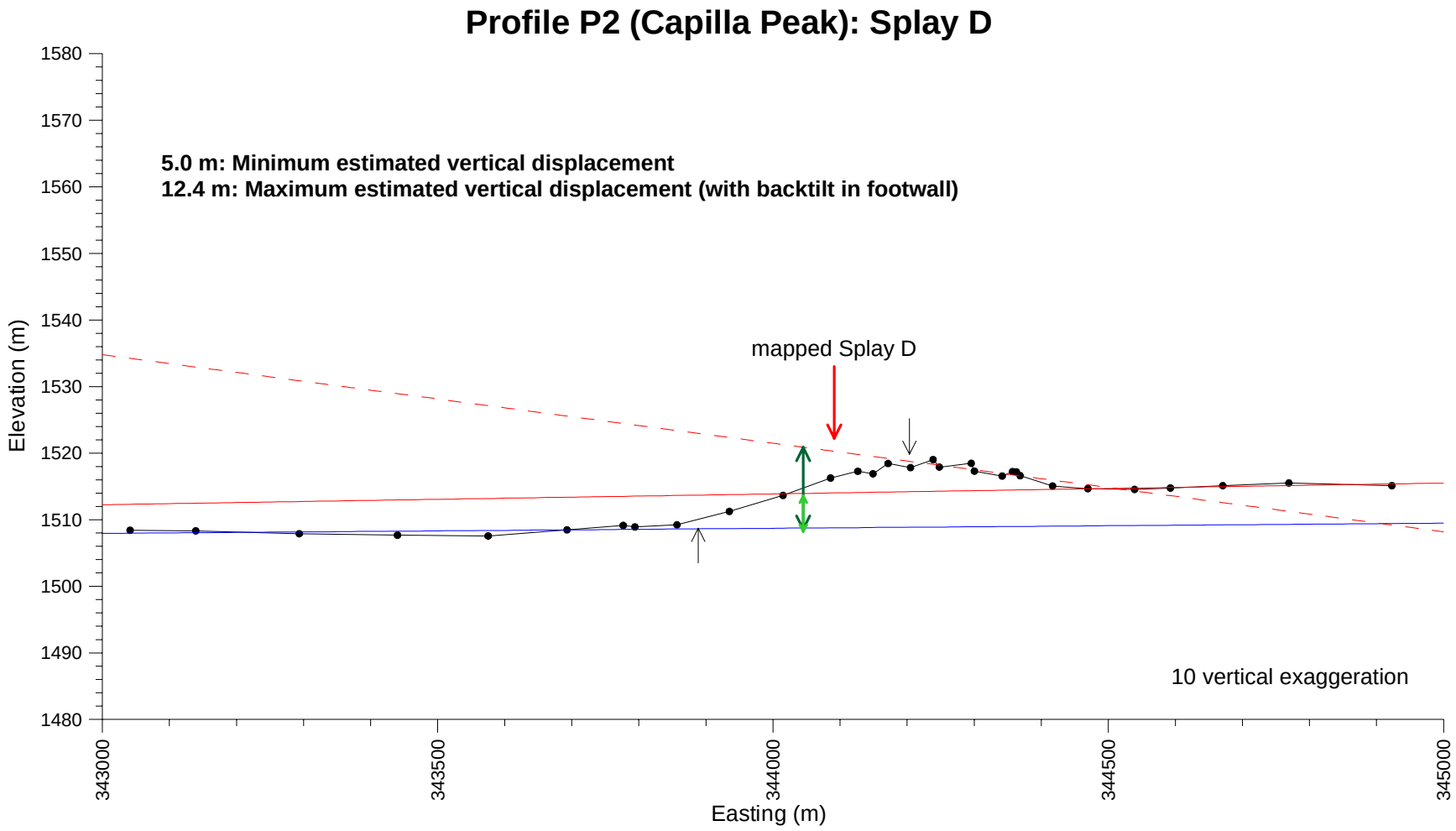

Figure 13. Vertically exaggerated section of Topographic Profile P2 at Fault Splay D. Estimates of net vertical surface displacements were measured midway between scarp crest and base (shown by gray arrows) at location of double-headed green arrows.

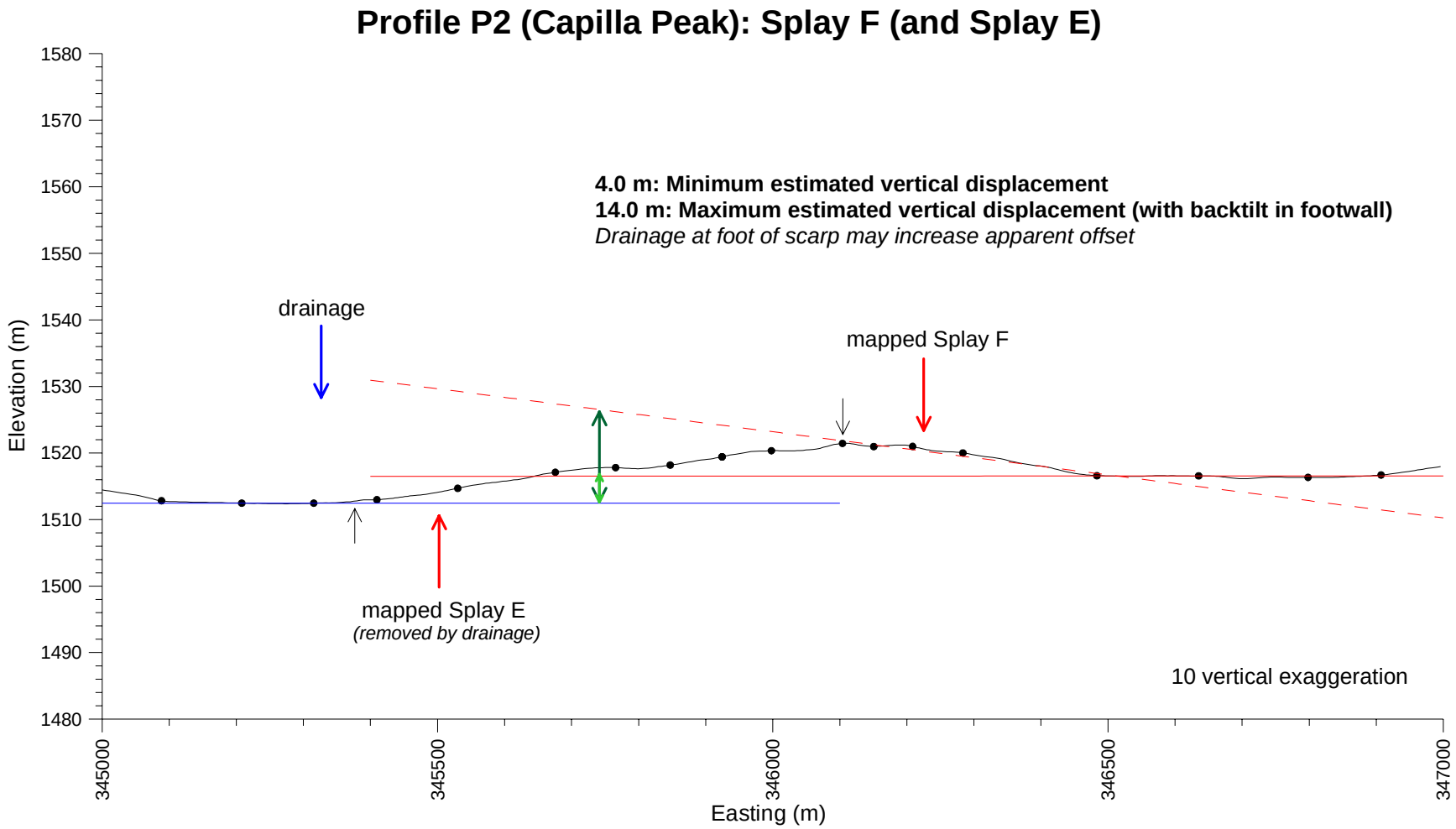

Figure 14. Vertically exaggerated section of Topographic Profile P2 at Fault Splays E and F. Estimates of net vertical surface displacements were measured midway between scarp crest and base (shown by gray arrows) at location of double-headed green arrows.

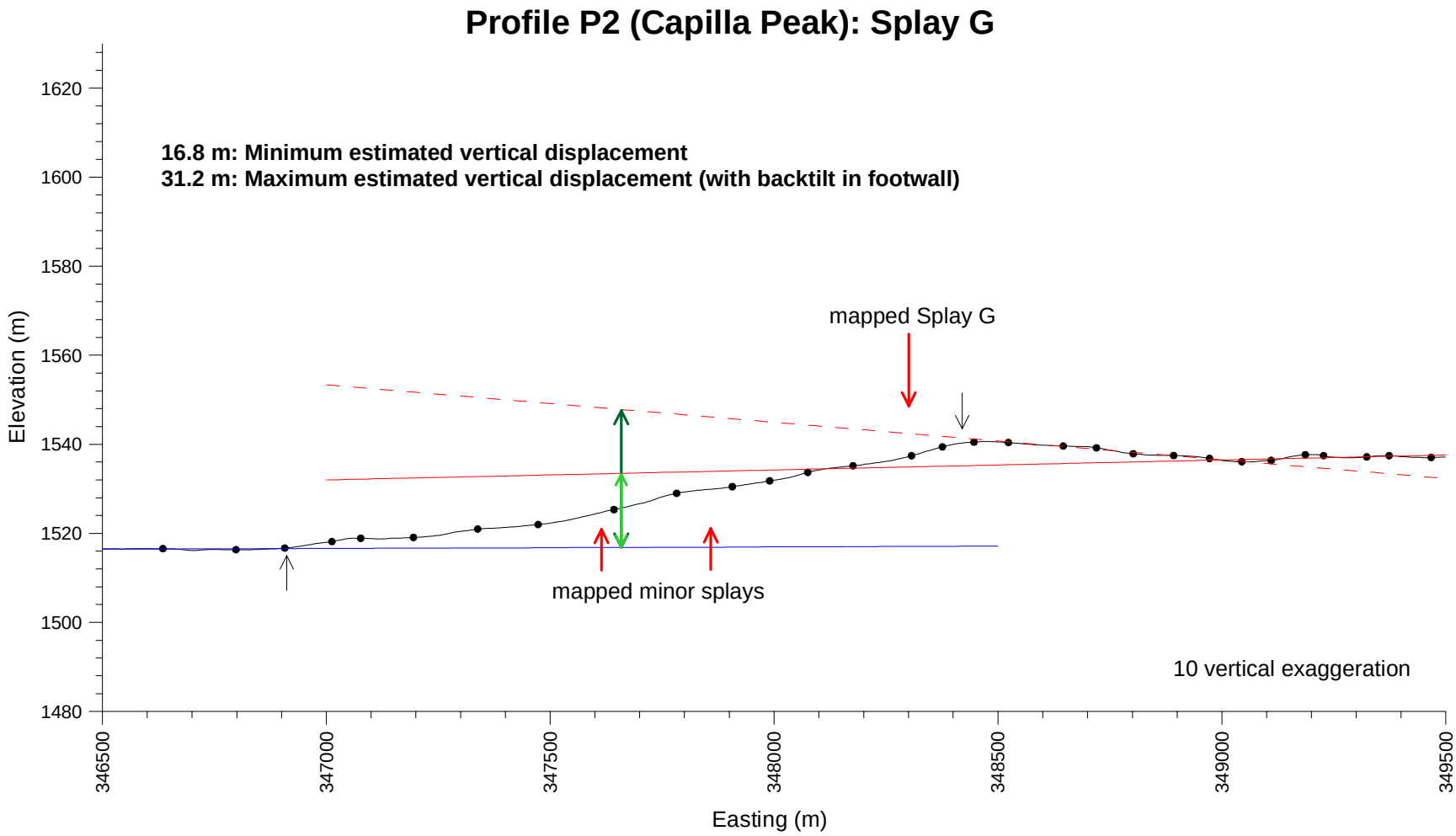

Figure 15. Vertically exaggerated section of Topographic Profile P2 at Fault Splay G. Estimates of net vertical surface displacements were measured midway between scarp crest and base (shown by gray arrows) at location of double-headed green arrows.

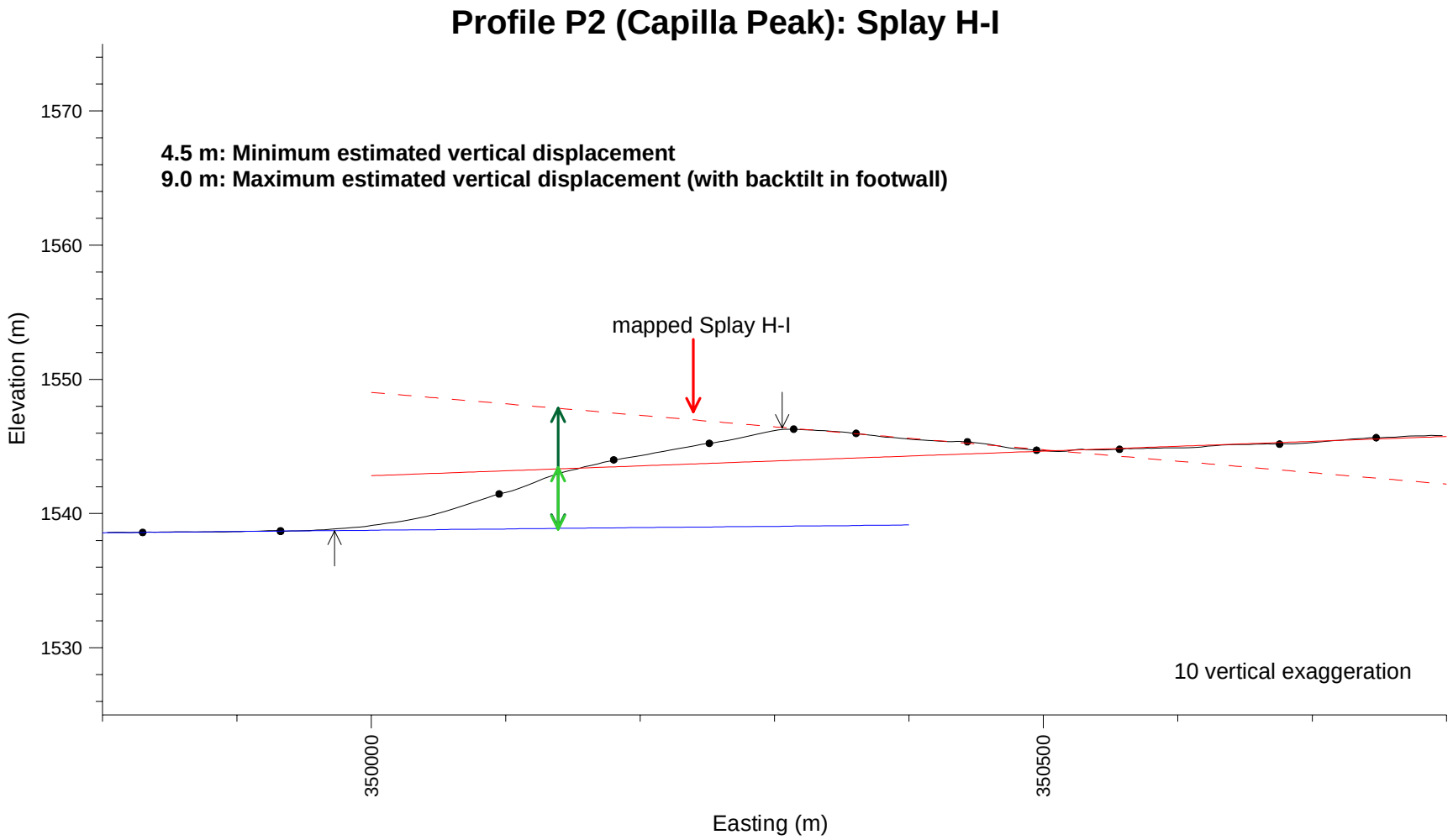

Figure 16. Vertically exaggerated section of Topographic Profile P2 at Fault Splay H-I. Estimates of net vertical surface displacements were measured midway between scarp crest and base (shown by gray arrows) at location of double-headed green arrows.

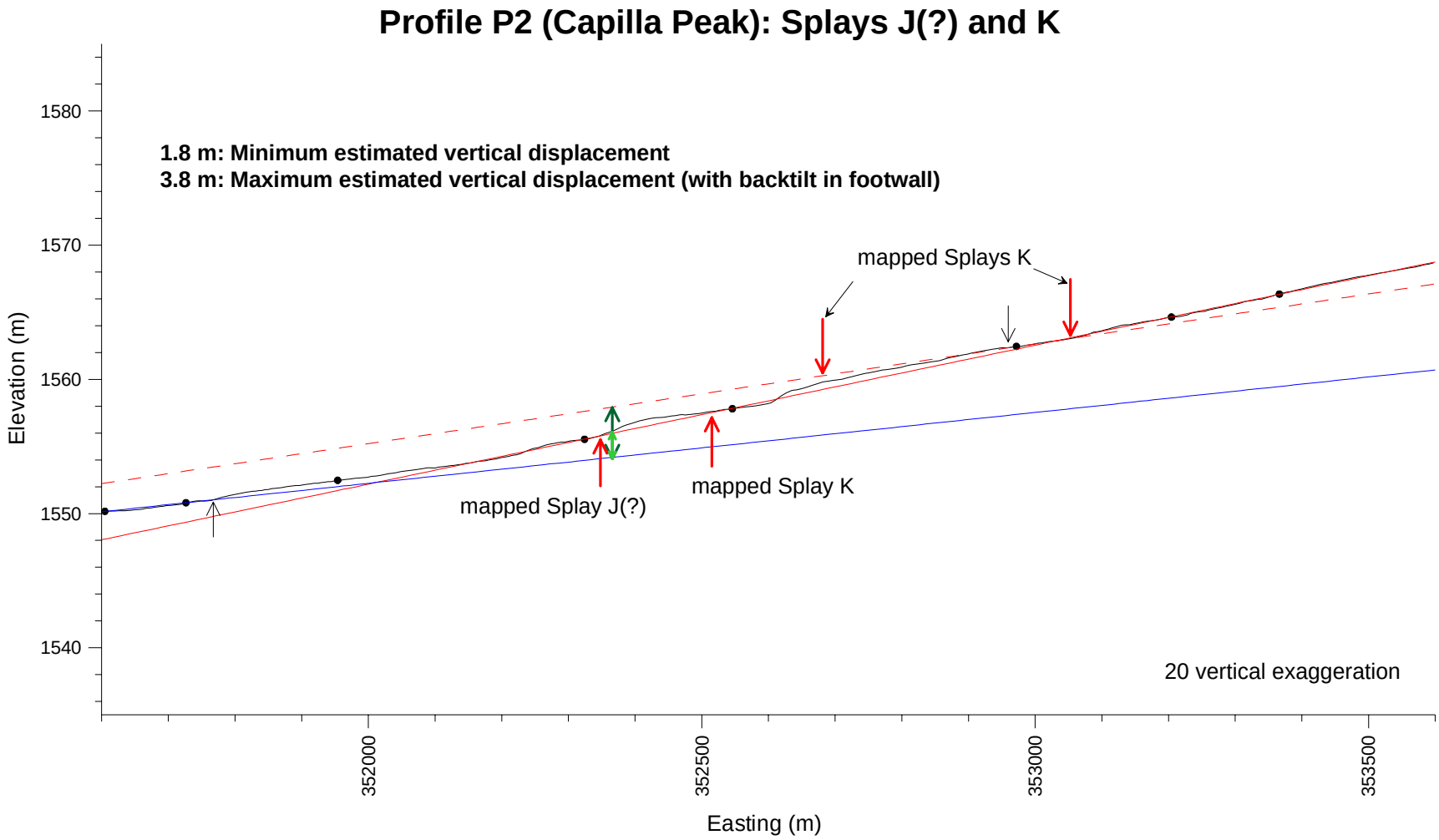

Figure 17. Vertically exaggerated section of Topographic Profile P2 at Fault Splays J(?) and K. Estimates of net vertical surface displacements were measured midway between scarp crest and base (shown by gray arrows) at location of double-headed green arrows.

Explanation

Study area boundary

Hubbell Spring fault system

- Quaternary fault scarp mapped in this study, dashed where uncertain or inferred, queried where highly uncertain, dotted where concealed; ticks on downthrown side; arrows show direction of backtilt
- Suspected Quaternary fault scarp (possibly non-tectonic) mapped in this study, dashed where uncertain or inferred, dotted where concealed; ticks on downthrown side
- Lineament (no scarp) mapped in this study
- Contreras Cemetery fault of McGraw et al., 2006, dashed where uncertain, dotted where concealed; ticks on downthrown side
- Faults modified from Maldonado et al. (2007) after Love et al. (1996) and Love (1998)
- Faults from the USGS Quaternary Fault and Fold Database including McCormick Ranch and Hubbell Spring faults (#2135 and #2120 of Machette et al., 1998) and modifications to the Palace Pipeline fault of Maldonado et al. (2007)

Other Quaternary faults

- Faults from the USGS Quaternary Fault and Fold Database, including:
  - 2033 Tijeras-Cañoncito fault system
  - 2037 Sandia fault
  - 2118 Los Piños fault
  - 2119 Manzano fault
  - 2121 Intra basin faults on the Llano de Albuquerque

Other features

- Trench sites
- P1 — Location of topographic profiles
- PH 2 — Photograph location
  - PH1: Figure 7a
  - Ph2: Figure 7b
  - PH3: Top cover photograph
  - PH4: Bottom cover photograph
- Boundaries of Tribal Lands of Isleta Pueblo and Sevilleta Wildlife Refuge
- Topographic quadrangle boundaries
- Municipal boundaries
- Roads

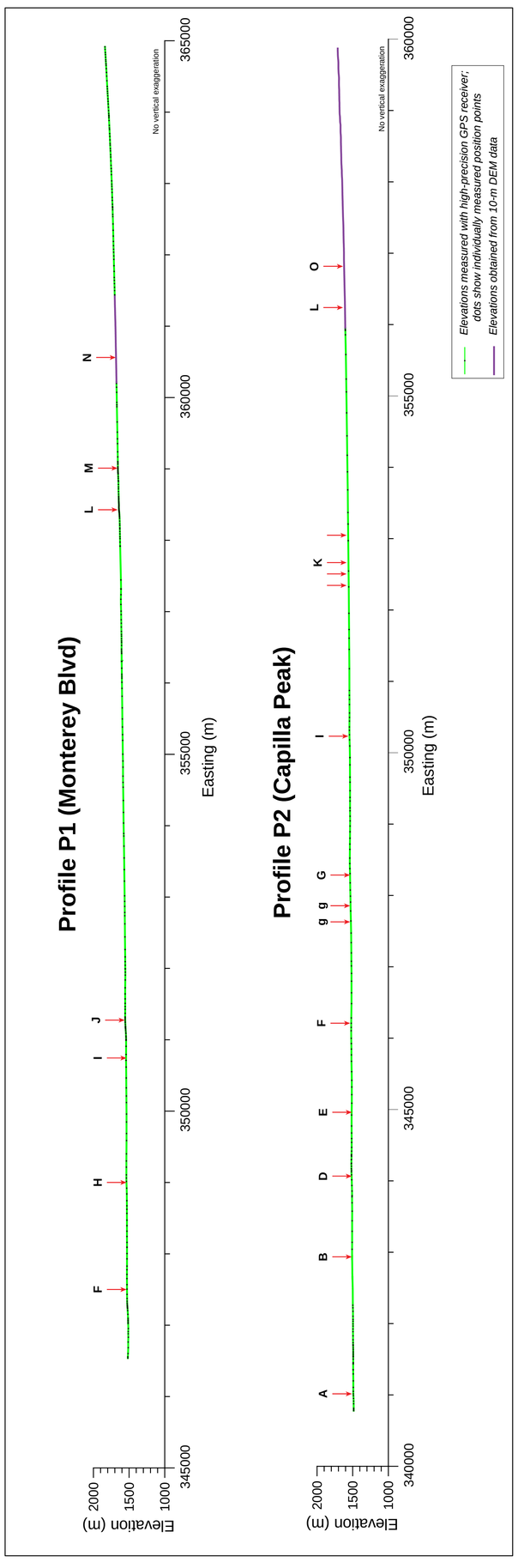

Base relief map derived from USGS NED 10-meter elevation data
Fault mapping by Judith Zachariasen and Susan Olig, 2005 to 2007

URS	Project No. 26814877 USGS NEHRP External Award 04HQGR0079: Additional analyses and mapping of the Hubbell Spring and other intrabasin faults south of Albuquerque, New Mexico	Map and Topographic Profiles of Quaternary Fault Scarps of the Hubbell Spring Fault System and Nearby Quaternary Faults, Southern Albuquerqe Metropolitan Area, New Mexico	Plate 1

W:\x_wcfs\PROJECTS\Llano de Manzano\Map_for_Report/Llano_fault_map_022608